Chemical Geology
August 2021, Volume 576 Pages 120278 (12p.)
https://doi.org/10.1016/j.chemgeo.2021.120278
https://archimer.ifremer.fr/doc/00691/80345/

Tropical mangrove forests as a source of dissolved rare earth elements and yttrium to the ocean

Dang Duc Huy [1, 2, *] , Zhang Zhirou [1], Wang Wei [1], Oursel Benjamin [3], Juillot Farid [4, 5], Dupouy Cecile [3, 5], Lemonnier Hugues [6], Mounier Stephane [7]

[1] Trent School of the Environment, Trent University, Peterborough, Canada
[2] Department of Chemistry, Trent University, Peterborough, Canada
[3] Aix Marseille Université, Université de Toulon, CNRS, IRD, MIO, Marseille, France
[4] Institut de Minéralogie, de Physique des Matériaux et de Cosmochimie, Sorbonne Université, UMR CNRS 7590, MNHN, ERL IRD 206, Paris, France
[5] Institut de Recherche pour le Developpement (IRD), Centre IRD Noumea, Nouvelle-Calédonie, France
[6] IFREMER, IRD, Université de la Nouvelle-Calédonie, Université de La Réunion, UMR 92200 ENTROPIE, Nouméa, Nouvelle-Calédonie, France
[7] Université de Toulon, Aix Marseille Université, CNRS, IRD, MIO, Toulon, France

* Corresponding author : Duc Huy Dang, email address : huydang@trentu.ca

Abstract :

Rare earth elements (REEs) and Y, or REYs, are commonly used as geochemical proxies for water chemistry, history of the continental crust and provenance studies. At the continent-ocean interface, the estuarine geochemistry of REYs is commonly thought to be driven by large-scale removal of the dissolved fraction. Consequently, contributions of river-borne dissolved REYs to the marine budget are assumed to represent a minor fraction of the total flux. Here, we report a significant release of dissolved REYs, together with a fractionation between light REEs, heavy REEs and Y, in the tropical mangrove estuaries of New Caledonia. These observations were associated with biogeochemical processes of the redox-dynamic mangrove system, rather than a possible contribution of REYs from a fresh groundwater source, based on stable water isotope compositions. These findings imply that tropical mangrove estuaries may act as a sizeable source of REYs to the ocean rather than buffer zones, at least for the dissolved fraction. We also extrapolated our data to compute the contributions of dissolved REY fluxes from the mangroves to global oceans. This preliminary calculation suggests that the mangrove system supplies 2.6-5% of global river-borne dissolved Nd, an REE with the most comprehensive mass balance. Therefore, given that the ocean mass budget of REYs remains unbalanced with fluxes missing on a global scale, considering the mangrove system as an input of oceanic mass balance models may help improve our understanding of the global distribution of REYs.

Graphical abstract

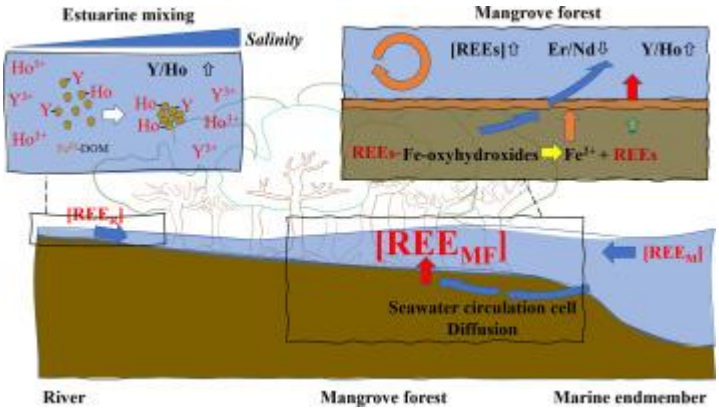

Highlights

► The mangrove forest acts as a source of dissolved REYs to the ocean. ► REYs are conservatively mixed in the mangrove estuary. ► Significant LREEs/HREEs and Y/REEs fractionation in the mangrove estuary ► The mangrove system supplies 2.6-5% of global river borne dissolved REYs.

Keywords : Rare earth elements, yttrium, water stable isotopes, mangrove, estuary

1. Introduction

Over the past decade, rare earth elements (REEs or the lanthanide series), Y and REE isotopes have received significant attention in geochemistry as tracers of the geological history of the continental crust and provenance study (Bayon et al., 2015). In paleoenvironmental studies, REEs are also commonly used as proxies to reconstruct water chemistry and oxygen saturation as per the distinct behaviour of Ce during redox transitions (Auer et al., 2017; Wallace et al., 2017). The fractionation between the light REEs (LREEs), heavy REEs (HREEs) and the non-lanthanide Y can also highlight the mechanisms of particle transport, sediment deposition and even geological features (e.g., iron formation) over the Earth's history (Bayon et al., 2015; Planavsky et al., 2010). More recently, because of the implication of REEs in novel technologies, REE anomalies (increased in concentrations of a specific REE relative to its neighbouring REEs) could also be used as a proxy for emission sources (Dang and Zhang, 2021; Ma et al., 2019; Tepe et al., 2014). However, the environmental chemistry of REEs remains fragmented, mostly regarding their anomalous behaviour across the river-estuarine-coastal water mixing zone where the fractionation between LREEs and HREEs is often associated with the redistribution of REEs among the dissolved and particulate fractions and the formation of stable dissolved complexes (Nozaki et al., 2000; Sholkovitz and Szymczak, 2000; Sholkovitz, 1995). As a consequence, the ocean mass budget of REEs remains unbalanced with missing fluxes at the global scale (Arsouze et al., 2009; Garcia-Solsona and Jeandel, 2020; Pourret and Tuduri, 2017; Tachikawa et al., 2003).

The interpretation of estuarine REE behaviour is fundamental to highlight their geochemistry at the continent-ocean interface. One conventional feature derived from decades of investigation on REEs' estuarine geochemistry is that large-scale removal of dissolved REEs (especially LREEs) occurs in the estuarine mixing zone (Elderfield and Greaves, 1982; Lawrence and Kamber, 2006; Nozaki et al., 2000; Pourret and Tuduri, 2017; Sholkovitz, 1995). This phenomenon minimizes the effective continental flux of REEs to the ocean and subsequently affects the marine budget calculations of REEs (Nozaki et al., 2000). Various factors would lead to such extensive removal of REEs. These include planktonic uptake, coprecipitation with ferromanganese oxyhydroxides and salt-induced coagulation of colloids (Hoyle et al., 1983; Nozaki et al., 2000; Sholkovitz and Szymczak, 2000). However, a limited number of publications pointed out a supply of dissolved

REEs in the mid-estuary zones (Lawrence and Kamber, 2006; Nozaki et al., 2000). This REE release could be associated with desorption from terrigenous suspended particles or remineralization in the estuarine system.

Moreover, most of the estuarine systems investigated so far for REEs geochemistry were major well-oxygenated riverine systems. However, it has been demonstrated that REEs cycling in marine waters can be impacted by redox variations (Bau et al., 1997). This process is particularly important as it can increase the effective continental REE flux to the oceans through enhanced supply to the water column upon dissolution of REEs-bearing oxyhydroxide phases. Therefore, further insights on REE behaviour across the redox-sensitive estuarine mixing zone are needed to strengthen our understanding of the REE geochemistry at the continent-ocean interface.

Tropical mangrove forests are of great interest to investigate these environmental conditions. First, they cover a large surface area (150,000 km^2) where complex hydrological processes balance abundant precipitation, surface runoff, and evaporation (Spalding, 2010). Moreover, the combination of elevated and annually constant temperature patterns with high bioavailability of natural organic matter boosts bacterial respiration, promoting hypoxia (Dubuc et al., 2019). To date, very limited studies on REEs focused on this critical ecosystem as it is generally assumed that the mangrove systems act as a buffer zone retaining trace elements and thus contribute a minor input for REEs to the oceans (Marchand et al., 2012).

Here, we investigated REE internal cycling within two estuarine mangrove systems in the subtropical region of New Caledonia. We meticulously measured dissolved REEs and Y over a 24-hour cycle in mangrove stations during a dry season and the spatial variations across the estuary in a rain season. To track whether additional water masses alter the mixing between the fresh and seawater endmembers, we also measured stable water isotopes ($\delta^{18}O$ and δD) to assess the hydrologic regime. We compared the stable water isotopes in these mangrove systems with other river waters collected in southeastern New Caledonia to verify the signature of the freshwater endmembers. Altogether, the data highlights REE behaviour during the estuarine mixing and document the mangrove forest's role on REE cycling at the continent-ocean interface. This dataset will help answer whether the REE continental flux from the tropical mangrove-dominated estuaries should be included in the REE marine budget.

2. Materials and Methods

2.1. Study site description

In the Southwest Pacific Ocean, New Caledonia is surrounded by the Coral Sea (**Figure 1A,B**). The main island "Grande Terre" is 400 km long and 64 km wide with a semi-arid tropical climate along the west coast. The whole island is also bordered by a coral reef enclosing a lagoon of over 20,000 km^2. The rich reef diversity and associated ecosystems were inscribed as a UNESCO World Heritage Site in 2008. On the other hand, most of the island is mountainous with vast ultramafic masses, schists and outcrops of basalt (Lillie and Brothers, 1970). Weathering of the ultramafic rocks' surface led to the formation of thick lateritic regoliths (tens of meters) hosting deposits of transition metallic elements of prime economic importance (Dublet et al., 2014; Noël et al., 2014). Between the lucrative mineral-rich land and the sea of tremendous ecological importance, the mangrove system acts as a buffer zone to filter heavy metals from reaching the reef (Marchand et al., 2012).

The hydrological behaviour of the Grande Terre is clearly distinct between the southwestern and northeastern coasts because of the 'rain-shadow' effect across the central massif divide (Terry and Wotling, 2011) (**Figure 1B**). Accordingly, the southwestern coast (leeward) tends to be drier than the windward northeastern coast. Overall, the hydrologic regime is characterized by high annual variability of rainfall amount and extreme events. Moreover, high and steep watersheds are associated with flash floods and thus rapid water transfer to the lagoons (Desclaux et al., 2018).

The Voh-Kone region (Northwest of the Grande Terre, **Figure 1B**) is an area of great economic and ecological interest. The Koniambo Massif hosts a large mine (Koniambo mine, **Figure 1C**), one of the largest nickel reserves in New Caledonia. The ore is conveyed to a coastal smelting site (Koniambo Nickel SAS, **Figure 1C**). Besides, the hydrologic system mainly comprises of two major rivers (Temala and Voh) discharging into the mangroves, then the bays of Chasseloup and Vavouto, respectively. Moreover, the hydrologic system comprises also of relatively smaller streams, such as the Coco River. These small tributaries have their flows significantly reduced during the dry season.

This study focused on the Temala and Coco Rivers (**Figure 1C**) in the Voh region. The Temala River originates from outside of the Koniambo Massif and discharges into Chasseloup Bay. It is, therefore, considered not impacted by mining activities. On the other hand, the Coco River's sources are in the Koniambo Massif hosting the Koniambo Mine. Along its course toward Vavouto Bay, the Coco River meanders parallelly to the ore conveyor. The Koniambo Nickel SAS smelting site is indeed only ca. 1.2 km away from the stream (**Figure 1 C**). Therefore, it is highly probable that this river is subject to anthropogenic impacts. Besides this contrasted exposition to anthropogenic sources, the natural geological settings of both rivers also differ. The Temala River catchement is made of soils developed on volcano-sedimentary rocks (cherts, basalts), whereas the Coco River catchment is composed of Ni-laterites developed on ultramafic rocks (peridotites) (Merrot et al., 2019).

We also investigated river waters (Dumbea, Coulee, Tontouta, Pirogue, **Table 1**) around Noumea in the Grande Terre's Southeast (**Figure 1B**) as a reference site for hydrological assessment using salinity and water isotope mixing.

2.2. **Water sampling**

We organized multiple sampling trips to investigate the hydrologic regime and REE cycling. The two first sampling campaigns were organized in June 2019 (dry season) and March 2020 (rain season) to collect samples in the Voh-Kone region (Temala and Coco Rivers). We also collected samples in four southeastern rivers (Dumbea, Coulee, Tontouta, Pirogue) in January, March, October and November of 2018. The March samples were collected during and after the Hola tropical cyclone while other samples are collected during the dry season.

During a dry season (June 2019), the first campaign aimed for a high-temporal resolution sampling in the mangrove forests (sites C2 and T6, hereafter referred to as "mangrove stations", **Figure 1C**). For that purpose, two automatic samplers (ISCO) were deployed during high tide (8-9h AM). The samplers were programmed to collect water samples one hour after installation to ensure the resettlement of resuspended sediments during deployment. The first water samples were collected at 9h AM at C2, and 10h AM at T6. Following samples were collected every hour. At the end of the 24-hour automatic sampling cycle, all samples were filtered (0.22 µm, cellulose acetate, Sartorius) directly on site. The filtered waters for stable water isotopes were filled to the

top to avoid water-air exchange, while samples for elemental analysis were acidified to pH<2 with ultra-trace HNO_3 (Merck). The samples were then immediately shipped by air to Trent University for analysis.

In 2020, during the rain season, a series of samples were collected across the salinity gradient along the Temala (T1-T8) and Coco (C1-C5) rivers (hereafter referred to as the "estuarine stations", **Figure 1C**). An additional sample was collected in the lagoon to serve as a marine endmember (M, **Figure 1C**). The samples were treated with the same protocol as in 2019 before being shipped to Trent University.

All the filters, sampling and storing bottles were previously rinsed with 10% HCl and milli-Q water (18 MΩ cm) in the laboratory and with river or lagoon water in the field.

2.3.**Water stable isotopes**

Water stable isotopes ($\delta^{18}O$ and δD, deuterium) were measured using a Liquid Water Isotope Analyzer (LWIA-24d, Los Gatos Research) at the Water Quality Center (Trent University, Ontario, Canada). The delta notation was calculated relative to the V-SMOW (Vienna-Standard Mean Ocean Water) standard.

$$\delta^{18}O = \left(\frac{\left(\frac{^{18}O}{^{16}O}\right)_{sample}}{\left(\frac{^{18}O}{^{16}O}\right)_{V-SMOW}} - 1 \right) \times 1000 (Eq.1)$$

$$\delta D = \left(\frac{\left(\frac{D}{^{1}H}\right)_{sample}}{\left(\frac{D}{^{1}H}\right)_{V-SMOW}} - 1 \right) \times 1000 (Eq.2)$$

Analytical recovery was assessed using two isotopic natural water reference materials (CRMs, Elemental Microanalysis, UK), covering the range of δ values found in natural waters (**Table S1**). Averages and standard deviations of each measurement (standards and samples) were calculated based on eight injections (i.e., n = 8, 750 nL each). We also used ultra-high purity water (18.2 MΩ cm) as an in-house standard to bracket every two samples to monitor analytical

drift and eliminate any memory effects. However, no correction was necessary. Analytical recovery of stable water isotopes is reported in **Table S1**.

2.4. Elemental analysis

To accurately determine the concentrations of REEs and Y at the ng/L levels in complex environmental matrices (seawater), we have performed a preconcentration step using column chromatography before analysis by Inductively Coupled Plasma Mass Spectrometry (ICP-MS). A full description of the REE column chromatography and ICP-MS analysis were reported elsewhere (Dang and Zhang, 2021; Ma et al., 2019). Briefly, REEs and Y in the filtered water samples were preconcentrated using 0.2 mL Nobias Chelate-PA1 resin (Hitachi High-Technologies). An aliquot of 50 mL of samples buffered at pH 6 was loaded on previously washed and conditioned resin. The seawater matrix was then washed off with 40 mL 0.05 M acetate buffer solution (pH = 6). REEs and Y were collected by eluting 20 mL of a 1 M HNO_3 solution through the column. This aliquot was collected into a 30 mL PTFE vessel and completely evaporated on a hotplate at 100^{o}C. A final 2 mL of 0.5 M HNO_3 was added to retake the REEs and Y.

All acids used to clean and wash the resins were double-distilled trace metal grade. The acetate buffer was also passed through the Nobias column for purification. We also meticulously checked procedural blanks and column recovery in every batch of 10 samples. Procedural blanks were between 0.1 to 29 pg of REEs and Y and significantly less than their mass in natural samples. Several aliquots (50 mL) of certified reference seawater CASS-6 (National Research Council of Canada, NRCC) were also repeated to test column recovery (Ma et al., 2019).

REEs and Y were determined using a triple quadrupole ICP-MS (8800 Agilent Technologies) at the Trent Water Quality Center. All REEs and Y were analyzed in MS/MS mode with O_2 as the reaction cell gas. Detection limits were in the range of 0.1-0.4 ng/L. Although there were no certified reference materials for REEs, we compared the REEs and Y concentrations measured in an NRCC natural water certified reference material (SLRS-6) to the values reported in a European interlaboratory calibration (Yeghicheyan et al., 2019). Excellent recovery was observed; the detailed data are reported in **Table S2**.

2.5. Normalization of REE patterns and calculations of anomalies

A common practice in the scientific community to eliminate the Oddo-Harkins effect and compare samples is to normalize the measured REE concentrations to geological materials (e.g., upper continental crust, shales, chondrite) or offshore seawater (Piper and Bau, 2013). Here, we normalized the measured concentrations of dissolved REEs to Post-Archean Australian Shale (PAAS (McLennan, 2001)) (Goldstein and Jacobsen, 1988; Ma et al., 2019; Piper and Bau, 2013). The shale-normalized concentrations are hereafter referred to as REE_{PAAS}.

In the current literature, excess or depletion of an REE relative to its neighbouring REEs are referred to as positive or negative anomaly of this element (REE/REE*). Accordingly, the REE anomalies could be determined by several approaches (e.g., arithmetic mean, geometric extrapolations, modelling the shape of PAAS-normalized patterns, third-order polynomial fit). Using all these approaches, Hatje et al. have demonstrated minor variability in the final results (Hatje et al., 2016). Therefore, we calculated Ce, Eu, and Gd anomalies using the following equations (arithmetic mean).

$$Ce/Ce^{*} = \frac{2 \times Ce_{PAAS}}{La_{PAAS} + Pr_{PAAS}} (Eq. 3)$$

$$Eu/Eu^{*} = \frac{2 \times Eu_{PAAS}}{Nd_{PAAS} + Sm_{PAAS}} (Eq. 4)$$

$$Ce/Ce^{*} = \frac{Gd_{PAAS}}{0.33 \times Sm_{PAAS} + 0.67 \times Tb_{PAAS}} (Eq. 5)$$

3. Results and Discussions

3.1. Physical-chemical properties

At both mangrove stations (C2 and T6, **Figure 1B**), pH values varied within a narrow range (7.8 ± 0.1, n = 48, **Table 1** and **Figure S1B**). Besides, the daily variations in salinity followed a sinusoidal curve, typical of estuarine systems (**Figure 2A**). This variation pattern is more noticeable at Temala with low tide (S = 26) recorded at 4h and 16h, and high tide (S = 33) at 22h. However, the salinity pattern at Coco is significantly distinct, with two events marked by steep drops at 13h, 19h and a third gradual decrease from midnight until 7h AM (1^{st}, 2^{nd}, 3^{rd} as marked in **Figure 2A**). The variation range of salinity in Coco is also narrower (29.6 to 34.2) than in Temala (26.0 to 33.0) (**Table 1**).

Temperature variations also help distinguish the two systems. Water temperatures increased from 16.8ºC at 11h and held constant at ca. 17.5ºC at Temala (**Figure S1A**, average of 17.3 ± 0.2ºC, n = 24, **Table 1**). However, the temperature pattern at Coco showed broader variations (15.5ºC to 16.5ºC, average of 16.1 ± 0.3ºC, n = 24, **Table 1**) with temperature drops at 11h and 21h (**Figure S1A**). Minimums in water temperatures at Coco are lagged by two hours relative to the salinity minimums (13h and 19h, **Figure 2A**).

Across the entire estuaries (estuarine stations), salinities ranged from 0 to 34.9 for the river water and marine endmembers, respectively (**Figure 2B**). On the other hand, all the river samples collected from the Southeast of New Caledonia are freshwater with a salinity of zero (**Figure 2C**).

3.2. Stable water isotopes and the hydrologic regime

The δD and $\delta^{18}O$ pairing. As the mangrove stations have narrow daily salinity variations (**Table 1**), so too is the range of stable water isotope compositions relative to the whole estuaries (**Figure 2 D-I**). At the mangrove stations, the δD-$\delta^{18}O$ relationship has the equation of $\delta D = 4.3 \times \delta^{18}O + 5.5$ (n=40, **Figure S2**). The slope of 4.3 ± 0.6 is typically lower than other tropical Pacific regions (5.1 to 6.5, Conroy et al. (2014)), and the global seawater average of 7.4 (Rohling, 2007). This indicates a strong influence of the evaporation process in the mangrove during the dry season.

Across the estuaries, the δD-$\delta^{18}O$ relationship of Coco and Temala waters aligns with southeastern rivers with the equation of $\delta D = 4.8 \times \delta^{18}O - 4.6$ (n=29, r^2=0.9, **Figure S2**). The slope (4.8 ± 0.3) is very similar to the mangrove stations (4.3 ± 0.6), only the intercepts differ (-5.3 across the estuary and +5.5 in the mangrove during the dry season).

According to the interpretation of the local evaporation line, as described by Wolfe et al. (2007), local surface waters often plot in linear clusters to the right of the Meteoric Water Line along a slope in the range 4 to 6. Our observations of consistent slopes (4.3 ± 0.6 and 4.8 ± 0.3) fall into this conventional interpretation (**Figure S2**) considering the Local Meteoric Water Line (LMWL) of $\delta D = 7.1 \times \delta^{18}O + 12.6$ (retrieved from the online isotopes in precipitation calculator, www.waterisotopes.org).

To explain the difference in the intercepts (higher values in the dry season than the rain season), we calculated the deuterium excess (d-excess) using the conventional approach: d-excess = $\delta D - 8\times\delta^{18}O$. This variable is valuable as it quantifies the deviation of a given dataset from the Global Meteoric Water Line (GMWL) by differential kinetic fractionation effects between D and ^{18}O. Such effects are related to humidity, moisture recycling and post-deposition process (Dansgaard, 1964). Low d-excess tends to reflect slow evaporation due to high humidity, while high d-excess values indicate fast evaporation due to low humidity (Lee et al., 2003). This interpretation is coherent with our observations as high d-excess values (15.8±1.3‰ and 15.9±2.9‰ at Coco and Temala, respectively) were observed at the mangrove stations in dry season while low d-excess values were typical of rain season and across the estuaries (0.4±5.8 ‰) (**Table 2**).

Pairing δD and $\delta^{18}O$ with salinity. The linear relationships between $\delta^{18}O$, δD and salinity have been used to estimate the stable water isotope composition of a freshwater endmember, defined as the $\delta^{18}O$ and δD values when salinity equals zero. This extrapolation should be interpreted with careful consideration of the contributions of regional precipitation, river water and runoff. However, it has been demonstrated that the extrapolated $\delta^{18}O$ and δD of freshwater endmembers in the Great Barrier Reef (NE Australia) reflected the isotope composition of local river water with relatively insignificant contributions of regional precipitation and runoff (Munksgaard et al., 2012).

Accordingly, $\delta^{18}O$ and δD values in the samples collected in the mangroves of Coco and Temala varied linearly with salinity (**Figure 3** and **Table 2**). In addition, all linear relationships converged to a common signature of the marine endmember (blue diamond in **Figure 3**). We extrapolated these linear relationships toward salinity of zero to determine the isotope composition of each river water endmember (**Table 2**). It is important to note that the interpretation of such relationships often requires a spatial and temporal assessment of the two systems (Conroy et al., 2017). As the samples were collected simultaneously in the dry season, the difference in water isotope composition between the freshwater endmembers at Coco and Temala can thus be only attributed to distinct water sources in each river system.

In the mangrove stations, the two linear regression lines are significantly distinct between Coco and Temala, except for a few stations at Temala that fall on the regression line of Coco (encircled

data, **Figure 3B**). These data represent the last samples collected during the high tide over the 24-hour series (3rd discharge event of the Coco River, **Figure 2A**). All physical-chemical properties and stable water isotopes of the two rivers overlap during this period (grey zone in **Figure 2 A, D, G**). This probably reflects a common blackish water mass formed during the high tide. Therefore, we excluded these data from Temala's δD-salinity regression because of the lack of more robust proxies to confirm this phenomenon and assuming that it may be minor. The exclusion of these three data did not affect the fact that the water isotope composition is significantly more depleted in the Coco River than Temala during the dry season. This depletion is more noticeable for δD (-72.9±8.9‰ vs. -36.0±2.8‰, respectively) than $\delta^{18}O$ (-9.9±1.7‰ vs. -8.4±1.2‰, respectively) (**Table 2**).

However, across the estuaries and during the rain season, the δD-S and $\delta^{18}O$-S relationships for both river systems are significantly similar ($p<0.05$) and align along with consistent equations ($\delta D=1.0\times S-33.7$ and $\delta^{18}O=0.2\times S-5.2$, **Table 2** and **Figure 3A**). Both the slopes and intercepts are close to the Temala mangrove during the dry season ($\delta D=1.0\times S-36.0$ and $\delta^{18}O=0.2\times S-8.4$, **Table 2**). This observation suggests that the hydrologic regime in the Temala River differs only slightly within seasons with relatively constant water isotope compositions of the river endmember ($\delta D_{River}^{Temala}$ ~ -34 to -36‰ and $\delta^{18}O_{River}^{Temala}$ ~ -5.2 to -8.4‰). These values are close to the four southeastern rivers over an annual cycle (**Figure 3A**) (δD_{River}^{SE}= -31 ± 6‰ and $\delta^{18}O_{River}^{SE}$ = -5.8 ± 1.0‰, **Table 2**), confirming reasonably consistent δD-S and $\delta^{18}O$-S relationships and hydrologic regimes of major river systems along the western coast of New Caledonia.

It is important to note that the Coco River is a small tributary with a relatively dry riverbed with significantly decreased flow during the dry season. Consequently, the Coco River's isotopic compositions differ substantially during the dry and rain seasons (**Table 2**) due to less precipitation and enhanced evapotranspiration during the dry season.

In summary, the difference in stable water isotope composition between the Coco and Temala rivers is related to the natural effects of a depleted hydrologic reservoir with enhanced evaporation. This effect is naturally more noticeable in small reservoirs during the dry season, such as the Coco River than the major streams (Temala and the four southeastern rivers). Overall,

we observed a relatively conservative hydrologic system with the mixing of only two water masses: the river freshwater and the marine endmembers. Water isotopic data allow excluding the contribution of a third water mass (e.g., groundwater discharge) in these mangrove-dominated estuarine systems.

3.3. **Rare earth element cycling in the mangrove system.**

The PAAS-normalized REE patterns are typical of coastal seawater with a gradual enrichment of heavy REEs relative to light REEs (Hoyle et al., 1983; Nozaki et al., 2000; Piper and Bau, 2013) (**Figure 4**). Moreover, we observed a depletion of Ce but an enrichment of Eu and Gd relative to their neighbouring REEs that are commonly referred to as anomalies. The anomalies of Ce and Eu were already extensively discussed in the literature. The negative Ce anomaly was shown to develop progressively with increasing salinity as dissolved Ce(III) undergoes continued oxidation to insoluble Ce(IV) across the estuarine zone (Nozaki et al., 2000). The positive Eu anomaly was also reported in the dissolved fractions of various major rivers (Amazon, St Lawrence, Piper and Bau, (2013)) and the clay fractions of river sediments worldwide (Bayon et al., 2015). Several previous studies have recorded positive Eu anomaly in continental materials (e.g., suspended load, atmospheric aerosol and dust, Censi et al., 2004; Goldstein and Jacobsen, 1988). Therefore, the positive Eu anomaly observed in the dissolved loads was interpreted as the result of dissolution from suspended particles and formation of stable dissolved complexes during transport (Nozaki et al., 2000).

On the other hand, the Gd anomaly is commonly associated with anthropogenic emissions, such as medical sources (medical resonance imagery) or wastewater (Hatje et al., 2016; Tepe et al., 2014). We observed Gd anomaly (Gd/Gd* up to 3.5) only during the dry season in the Coco river, in the first and second freshwater discharge events (**Figure S3** and **Figure 2A**). We have previously suggested that the 3rd event may be associated with a common brackish water at both Coco and Temala rivers formed during the high tide from 4h to 9h AM (**Figure 2A**), which is Gd-anomaly-free (**Figure S3D**). No Gd anomaly (Gd/Gd* = 1) was indeed observed in the marine endmember (blue diamonds, **Figure 4 C,D**). Given the absence of major medical facilities and considering the low population along the Coco river, a possible medical or wastewater origin for this Gd anomaly can be ruled out. However, the Coco River is associated with the nickel mined lateritic Koniambo regolith where a 13km long ore conveyor was built parallel to the river

and the Koniambo Nickel SAS smelting plant is adjacent to the Coco mangrove (**Figure 1C**). While there is no precedent study reporting Gd anomaly associated with lateritic ores extraction and processing, the Gd anomaly observed in the Coco river might be associated with those activities.

Estuarine mixing behaviors of REEs and Y. The REE concentrations in the marine endmembers are typically low; the sum of all REE concentrations (ΣREEs) approximates 6 ng/L. However, there was a significant difference in REE total concentrations between the two river endmembers, with Temala containing more REEs than Coco (ΣREEs of 24 and 2.6 ng/L, respectively). This trend was also observed at the mangrove stations (**Figure S3A**). The higher REE concentrations measured in the Temala River waters compared to the Coco River are directly associated with the geology of their watersheds. The Temala watershed is indeed made of soils developed on volcano-sedimentary rocks, whereas the Coco river meanders on lateritic soils developed on ultramafic rocks (**Figure 1C**) (Merrot et al., 2019). As volcaniclastic bedrock tend to contain higher REE and Y concentrations than the granitic regolith (Chapela Lara et al., 2018), the difference in the watershed's geology could be directly associated with higher REE concentrations in Temala river waters than Coco.

Moreover, we did not observe any REEs and Y removal during estuarine mixing between the rivers and the marine endmember, as commonly assumed for REE estuarine geochemistry (see section 1). In fact, we measured very high REE concentrations in the mangrove forest (salinity range of 25-33, see La concentrations in **Figure 5A**). The high REE (La) concentrations in the mangrove area seem to be conservatively mixed with the freshwater mass ($y=0.6x+3.5$, $r^2 = 0.97$) and the marine endmember ($y=-5.2x+183$, $r^2 = 0.84$). This situation was not reported previously. It is commonly assumed that approximately 60-90% of REEs are removed from the low salinity region of an estuary by flocculation/coagulation of dissolved organic-bound Fe and colloidal materials depleting REEs from the dissolved pool (Lawrence and Kamber, 2006; Pourret and Tuduri, 2017; Sholkovitz and Szymczak, 2000; Sholkovitz, 1995). Minor releases of REEs during an estuary mixing were only reported in the turbid-clear water transition zone (S=12-15) in the Chao Phraya estuary (Thailand) (Nozaki et al., 2000) and the mid-salinity zone of the Elimbah Creek (Australia) (Lawrence and Kamber, 2006). Such REE release was attributed to several mechanisms, including desorption from suspended particles, coastal erosion, and

mineralization during early diagenesis. In addition, the reductive dissolution of ferromanganese oxides has been shown to significantly release REEs into the porewater, although LREEs tend to sorb back onto the newly formed ferromanganese oxides at the sediment-water interface (Och et al., 2014).

Although the La-salinity biplots (**Figure 5A**) could be interpreted as mixing of three water masses (river, mangrove forest, and marine), stable water isotopes (**Figure 3**) allow to rule out the possibility of a third water mass in the estuaries of Coco and Temala. Thus, the high La concentrations in the mangrove are instead explained by specific biogeochemical processes leading to the substantial release of dissolved REEs. Given the subtropical weather condition and the high availability of fresh organic matter in the mangrove forest (Noël et al., 2014), it is highly probable that bacterial activity contributes to this REEs solubilization in the sediments porewater (Och et al., 2014). In the mangrove system, the tidal conditions with water pushing up through the porous sediment (seawater circulation cell, **Figure 6A**) would then favour REE remobilization to the water column. A previous study has demonstrated significant fluxes of REEs from such a seawater circulation through diagenesis-active sediments (i.e., organic matter degradation and reductive dissolution of ferromanganese oxides (Paffrath et al., 2020), **Figure 6**). Other processes such as passive diffusion fluxes or sediment resuspension events induced by waves and tides (Dang et al., 2020) or bioturbation could also contribute to the REE release towards the water column (**Figure 6 C**). At a larger scale of the Northwestern Mediterranean Sea, upward diffusion of REEs (Nd) from sediment porewater counts for 30% of the Nd marine budget (Garcia-Solsona and Jeandel, 2020). Moreover, given the organic mater-rich surface waters in the mangrove system and the high affinity between REEs and dissolved organic carbon (Davranche et al., 2004; Marsac et al., 2010; Pourret and Davranche, 2013), it is also highly possible that the formation of stable organic complexes could contribute to maintaining REEs in solution in this mid-salinity region (25-33).

Fractionation of HREEs/LREEs and elemental ratios. All the water samples collected showed a progressive enrichment of HREEs relative to the PAAS shale (**Figure 4**). This is consistent with the conventional REE behaviours in the aquatic environment where the fractionation between the dissolved and particulate loads of HREEs and LREEs leads to this characteristic REE curve (Piper and Bau, 2013). Therefore, elemental ratios between representative HREEs and

LREEs (e.g., Er/Nd (Nozaki et al., 2000), Nd/Lu (Sholkovitz, 1995), Ho/Er (Lawrence and Kamber, 2006)) could help determine whether this fractionation occurs in the freshwater endmember or the estuary. As the interpretations using different ratios are very similar, we choose to discuss only the Er/Nd (weight ratios).

The Er/Nd ratios in both UCC (Rudnick and Gao, 2003) and PAAS (McLennan, 2001) approximate 0.08, while those in the river endmembers are significantly above this value (0.2 and 0.3 at Temala and Coco, respectively, **Figure 5B**). This indicates that the fractionation between HREEs and LREEs occurred in the freshwater system. It is important to note that such fractionation is pH-dependent. At the pH range observed in Temala and Coco rivers (7.7-7.9, **Table 1**), REE adsorption on particles is enhanced, leading to significant fractionations by preferential LREE removal (Sholkovitz, 1995). Furthermore, the measured Er/Nd in the estuarine samples varied with salinity along the conservative mixing line of Temala (**Figure 5B**), suggesting no further fractionation (Lawrence and Kamber, 2006). This is consistent with the occurrence of dissolved organic-REE complexes in the mangrove waters, as previously suggested. Previous studies have demonstrated that the presence of dissolved organic matter significantly reduced REE sorption on ferromanganese oxides and the subsequent fractionation between LREEs and HREEs (Davranche et al., 2005, 2004).

On the other hand, a negative departure from the conservative mixing line (i.e., Er/Nd ratios decreased) was noticed at the mangrove stations (black arrow in **Figure 5B**). This indicates a preferential release of LREEs (Nd) relative to the HREEs (Er). This observation is in agreement with the hypothesis that LREEs previously bound to the solid fraction are released toward solution when the oxide phases undergo reductive dissolution (Bau et al., 1997). High REEs concentrations in porewater promote upward diffusion from the sediments by the seawater circulation cell or diffusive flux (**Figure 6**).

Furthermore, variations in the Y/Ho ratios are also of great interest. Although these two elements have similar ionic radii, their electronic configurations differ. Yttrium has no f-electron while Ho has 10 electrons filling up the f orbitals (Lawrence and Kamber, 2006). Therefore, the ability to form strong surface and solution complexes using the f orbitals (Byrne and Lee, 1993) drives the fractionation of this pair during weathering, riverine transport or in the marine environment

(Lawrence and Kamber, 2006; Nozaki et al., 2000). As a result, Ho tends to form more stable surface complexes than Y (Bau et al., 1997; Byrne and Lee, 1993; Lawrence and Kamber, 2006). Therefore, two conditions could lead to Y/Ho fractionation during estuarine mixing. First, coagulation, flocculation and sedimentation of Ho-bearing colloidal particles preferentially remove Ho from solution. Second, as Y tends to form weaker surface complexes than Ho, this fractionation is enhanced by the salt effect (competition for surface sorption sites), which favors Y release from colloidal particles toward solution. Both processes were well documented in the literature to support the increase in the Y/Ho ratio during the estuarine mixing (**Figure 6B**) (Lawrence and Kamber, 2006).

The Y/Ho ratio in the Temala river endmember (28.4) approximates UCC and PAAS (25.3 (Rudnick and Gao, 2003) and 27.2 (McLennan, 2001), respectively), indicating that there was no significant fractionation between Y and the REEs in the Temala river (**Figure 5C**) (Lawrence and Kamber, 2006). However, in the Coco river endmember, the Y/Ho ratio is significantly lower (18.6). A situation where Y-Ho fractionation leads to lower Y/Ho ratios relative to the UCC is scarcely reported in the literature. While considered a minor process in natural water systems, it was previously reported by Bau et al. in the slightly acidic solutions of low complex-forming capacity of a stream from an abandoned mine (Bau et al., 1995). Interestingly, the Coco River, where this phenomenon is suspected to occur, is connected to the Koniambo mine.

In the estuary, we also observed the conventional Y/Ho fractionation (**Figure 6B**) as the Y/Ho ratios were beyond the conservative mixing lines (**Figure 5C**). However, the positive departure is even more noticeable in the mangrove forest, with Y/Ho reaching up to 80 (black arrow in **Figure 5C**). This suggests that additional processes took place in the mangrove forest area, further fractionating this pair. A previous study has suggested that the fractionation between Y and Ho could be redox driven (Bau et al., 1997). Accordingly, a redox change is expected to occur at the sediment-water interface (**Figure 6C**) where the upward diffusive flux from mangrove sediments confronts the freshly formed ferromanganese oxyhydroxides. As discussed previously, these reactive surfaces tend to further remove Ho relative to Y. Such preferential removal of Ho increases the Y/Ho ratios as observed in **Figure 5C**.

3.4. Calculations of REE flux from the mangrove systems

Fluvial fluxes of dissolved constituents in the oceans are essential to balance their marine budget. The current ocean box models for REEs consider major inputs as river-borne dissolved and particulate load, atmospheric dust, groundwater discharge, porewater diffusion and dissolution of reworked sediments (Arsouze et al., 2009; Garcia-Solsona and Jeandel, 2020; Tachikawa et al., 2003).

Goldstein and Jacobsen have suggested a simple empirical approach to calculate the dissolved REEs flux ($R_i^{eff.}$) from the continent (Goldstein and Jacobsen, 1988) as detailed in the following equation.

$$R_i^{eff.} = C_i^R \times F_R \times \phi_i \times CF \quad (Eq. 6)$$

where C_i^R is the dissolved concentration of an element in the continental endmember (ng/L), F_R is the annual river discharge, Φ_i is the effective factor, and CF is a correction factor to convert the final units into kg/year.

Here, we applied this calculation to our preliminary dataset to determine whether the fluxes of REEs and Y from the tropical mangrove system could be of interest in the global oceanic budget. Therefore, it is important to note a few assumptions in this simple calculation. First, because of the conservative mixing of REEs and Y between the mangrove system and the seawater (**Figure 5A**), we can assume a full effective factor (i.e., absence of estuarine removal or Φ_i =1). Second, the local Water Agency (DAVAR, Service de l'eau) monitored the hydrologic regime of the local river systems. According to the most recent report, the monthly discharges of the rivers in the leeward side (southwestern, e.g., Boghen, Poya, Pouembout-Boutana Rivers) of Grand Terre in 2019 and 2020 average 18.6 m^3/s in February and 0.6 m^3/s in May (the month preceding the two sampling campaigns) (DAVAR Service de l'eau, 2020). The variability of the river discharge that could differ Coco and Temala, although not individually determined, could be consisted within the variability of major river systems of the leeward sides. Third, the concentrations of REEs and Y of the mangrove endmember (C_i^R) are those of the samples with salinity in the range of 25-34 (the mangrove forest, **Figure 5A**). Finally, the calculated fluxes ($R_i^{eff.}$) of dissolved REEs and Y from the mangrove system are reported with standard deviations reflecting the errors propagating through the calculations and variability of all variables.

Accordingly, $R_i^{eff.}$ values of Temala and Coco in the dry and rain seasons are reported in **Table S3** while the annual average fluxes are showed in **Table 3**. The fluxes of REEs and Y are significantly higher in the rain season and dry season (**Table S3**), as reported in other major estuarine systems (Pourret and Tuduri, 2017). Overall, the annual averages of REE and Y fluxes from the Coco and Temala range from 0.05 (Lu) to 16.1 (Y) kg per year (**Table 3**).

To extrapolate our data toward a general perspective of the global mangrove system, we first normalized the calculated fluxes to mangrove watershed surface areas (S_W, km^2) and the fraction of vegetation coverage (f_V). Equation 7 allows the calculation of area-normalized fluxes of REEs and Y from the two mangrove forests (R_i^{S-MF}, $kg/yr/km^2$).

$$R_i^{S-MF} = \frac{R_i^{eff.}}{S_W \times f_V} (Eq. 7)$$

The watershed of the Voh region has a vegetation coverage of approximately 43±16% (Taureau et al., 2019), thus f_V =0.43. The surfaces of the Temala and Coco watersheds (S_W) approximates 163 km^2 and 42 km^2, respectively (FalconBridge NC, 2001). The calculated area-normalized fluxes of REEs and Y range from 1.6×10^{-3} (Lu) to 0.4 (Y) $kg/yr/km^2$.

From the R_i^{S-MF} values, we attempted an extrapolation to the global surface of mangroves (150,000 km^2) (Spalding, 2010) and thus calculated the global fluxes of dissolved REEs and Y from this unique ecosystem (**Table 3**). These global fluxes calculated for the mangrove systems could then be compared to the published global river-borne dissolved Nd loads (Arsouze et al., 2009; Garcia-Solsona and Jeandel, 2020; Tachikawa et al., 2003). Currently, the Nd oceanic budget is the most comprehensive as extensive studies reported both Nd concentrations and isotope composition to calibrate its ocean box models. In these models, the river inputs of dissolved Nd range from 260 to 500 tons per year (or Mg per year) (Rousseau et al., 2015; Tachikawa et al., 2003). Relative to these values, we estimate that the mangrove systems supply 13.3±5.6 tons per year of dissolved Nd, representing 2.6-5 % of the total river input of dissolved Nd. Compared to other sources (e.g., dust dissolution of 400 tons of Nd per year, Nd release from suspended particles of 5,700±2,600 ton per year) (Arsouze et al., 2009; Rousseau et al., 2015; Tachikawa et al., 2003), the mangrove systems appear to be a minor source. However, it is important to note that even though this study documents a significant release of REEs and Y

within the mangrove system for the first time, we assess only two small mangrove systems representing <1% of the global mangrove surface. Further studies are therefore required to better characterize the contribution of the mangrove system to the global marine budget.

4. Implications for the role of mangrove on REE cyling and oceanic budgets.

The conventional estuarine REE behaviour often implies a sharp removal of REEs when a riverine water mass enters an estuary. However, our data revealed a significantly release of dissolved REEs and Y (7.3 times for Y, 6.4 times for La and 3.3 times for Lu) in the mangrove system. Although other water masses could supply REEs to the water column (e.g., groundwater discharge (Kim and Kim, 2011)), our stable water isotopes data confirm a sole binary mixing between the fresh and seawater endmembers in the mangrove estuaries of New Caledonia. This release of REEs and Y has thus to be associated only with internal recycling or biogeochemical processes within the mangrove forests. This dataset thus strengthens the hypothesis that tropical mangroves act as a source of dissolved REEs and Y to the marine system.

This finding first redefines the role of tropical mangroves in the cycling of trace elements at the continent-ocean interface. While mangrove forests are often referred to as a buffer zone to filter trace metals from reaching the open sea (Marchand et al., 2012), this assumption might be valid only for the particulate loading. This specific ecosystem produces large amounts of organic matter that is bioavailable for bacterial degradation (Marchand et al., 2012) and thus boosts early diagenesis. These biogeochemical processes lead to the complex recycling of REE-bearing phases. The reductive dissolution of ferromanganese oxides occurs within the subsurface layers of the sediments and is thus responsible for releasing trace elements (Dang et al., 2015, 2014). However, the redox boundary at the seawater-sediment interface leads to forming a thin layer of newly formed Fe- and Mn-oxyhydroxides with large reactive surface areas that efficiently sorb trace elements and thus minimize their upward diffusive flux (Dang et al., 2015; Rigaud et al., 2013). Although we could not evaluate the relative amounts of REEs being diffused upward from the sediment porewaters relative to REEs retained at the interface, the diel variation in oxygen concentrations associated with hypoxia events in the mangrove (Dubuc et al., 2019) strongly suggests that the fraction of REEs being retained would be minor regarding the low stability of Fe- and Mn-oxyhydroxides in such redox-dynamic conditions (Bau et al., 1995).

Over the past 30 years, several works aimed to understand and revisit REE behaviour during estuarine mixing and accumulation in sediments (Bayon et al., 2015; Lawrence and Kamber, 2006; Sholkovitz and Szymczak, 2000; Sholkovitz, 1995). This first dataset reporting REEs release in a tropical mangrove may provide an important insight into the contribution of mangrove forests to the oceanic budgets and mass balance of REEs and Y. However, these box models remain unbalanced with a significant missing flux (e.g., 800 Mg per year) (Tachikawa et al., 2003). Pourret and Tuduri (2017) recently suggested the continental shelves as a potential resource of REEs to be included in the oceanic mass balance of REEs. Moreover, mangrove is growing in 123 tropical and subtropical countries and covers a total surface of 150,000 km^2 (Spalding, 2010). Our simple flux calculation suggests that this atypical system supplies a significant proportion of REEs toward the oceans (2.6-5% of the global dissolved loading). However, it remains uncertain about the representativity of the Coco and Temala systems of the global mangroves. Therefore, further research on the REE cycling within mangrove systems is needed to determine whether the mangrove estuaries should be considered a significant input in ocean mass budget to balance the global REE distribution.

Aknowledgements: The authors thank the Trent University's Internal Operating Grant (#26090) for financial support to D.D.H. Besides, C.D., F.J., H.L., S.M. and B.O. also acknowledge funding from CRESICA (grant CDEI 2017-2021 - VI-3), CDEI 2017-2021 - VI-3 (grant EC2CO-Bioeffect/Ecodyn/Dril/MicrobiEn ''TREMOR'') and CNRT (grant CSF 9PS2013 ''DYNAMINE''). We also wish to thank Florence Royer (Ifremer) and Etienne Lopez (Ifremer) for their technical assistance during freshwater sampling in the south, as well as the technical (LAMA, US IMAGO) and administrative staff at IRD Noumea for their help and support relative to field campaigns.

References

Arsouze, T., Dutay, J.-C., Lacan, F., Jeandel, C., 2009. Reconstructing the Nd oceanic cycle using a coupled dynamical – biogeochemical model. Biogeosciences Discuss. 6, 5549–5588. doi:10.5194/bgd-6-5549-2009

Auer, G., Reuter, M., Hauzenberger, C.A., Piller, W.E., 2017. The impact of transport processes

on rare earth element patterns in marine authigenic and biogenic phosphates. Geochim. Cosmochim. Acta 203, 140–156. doi:10.1016/j.gca.2017.01.001

Bau, M., Dulski, P., Moller, P., 1995. Yttrium and holmium in South Pacific seawater : vertical distribution and possible fractionation mechanisms. Chemie der Erde - Geochemistrymie der Erde 55, 1–15.

Bau, M., Moller, P., Dulski, P., 1997. Yttrium and lanthanides in eastern Mediterranean seawater and their fractionation during redox-cycling. Mar. Chem. 56, 123–131.

Bayon, G., Toucanne, S., Skonieczny, C., André, L., Bermell, S., Cheron, S., Dennielou, B., Etoubleau, J., Freslon, N., Gauchery, T., Germain, Y., Jorry, S.J., Ménot, G., Monin, L., Ponzevera, E., Rouget, M.L., Tachikawa, K., Barrat, J.A., 2015. Rare earth elements and neodymium isotopes in world river sediments revisited. Geochim. Cosmochim. Acta 170, 17–38. doi:10.1016/j.gca.2015.08.001

Byrne, R.H., Lee, J.H., 1993. Comparative yttrium and rare earth element chemistries in seawater. Mar. Chem. doi:10.1016/0304-4203(93)90197-V

Censi, P., Mazzola, S., Sprovieri, M., Bonanno, A., Patti, B., Punturo, R., Spoto, S.E., Saiano, F., Alonzo, G., 2004. Rare earth elements distribution in seawater and suspended particulate of the Central Mediterranean Sea. Chem. Ecol. 20, 323–343. doi:10.1080/02757540410001727954

Chapela Lara, M., Buss, H.L., Pett-Ridge, J.C., 2018. The effects of lithology on trace element and REE behavior during tropical weathering. Chem. Geol. 500, 88–102. doi:10.1016/j.chemgeo.2018.09.024

Conroy, J.L., Cobb, K.M., Lynch-Stieglitz, J., Polissar, P.J., 2014. Constraints on the salinity-oxygen isotope relationship in the central tropical Pacific Ocean. Mar. Chem. 161, 26–33. doi:10.1016/j.marchem.2014.02.001

Conroy, J.L., Thompson, D.M., Cobb, K.M., Noone, D., Rea, S., Legrande, A.N., 2017. Spatiotemporal variability in the δ18O-salinity relationship of seawater across the tropical Pacific Ocean. Paleoceanography 32, 484–497. doi:10.1002/2016PA003073

598 Dang, D.H., Layglon, N., Ferretto, N., Omanović, D., Mullot, J.-U., Lenoble, V., Mounier, S.,
599 Garnier, C., 2020. Kinetic processes of copper and lead remobilization during sediment
600 resuspension of marine polluted sediments. Sci. Total Environ. 698, 134120.

601 Dang, D.H., Lenoble, V., Durrieu, G., Mullot, J.-U., Mounier, S., Garnier, C., 2014. Sedimentary
602 dynamics of coastal organic matter: An assessment of the porewater size/reactivity model by
603 spectroscopic techniques. Estuar. Coast. Shelf Sci. 151, 100–111.
604 doi:10.1016/j.ecss.2014.10.002

605 Dang, D.H., Lenoble, V., Durrieu, G., Omanović, D., Mullot, J.-U., Mounier, S., Garnier, C.,
606 2015. Seasonal variations of coastal sedimentary trace metals cycling: Insight on the effect
607 of manganese and iron (oxy)hydroxides, sulphide and organic matter. Mar. Pollut. Bull. 92,
608 113–124. doi:10.1016/j.marpolbul.2014.12.048

609 Dang, D.H., Zhang, Z., 2021. Hazardous motherboards: Evolution of electronic technologies and
610 transition in metals contamination. Environ. Pollut. 268, 115731.

611 Dansgaard, W., 1964. Stable isotopes in precipitation. Tellus. doi:10.3402/tellusa.v16i4.8993

612 DAVAR Service de l'eau, 2020. Synthèse Ressource en Eau.

613 Davranche, M., Pourret, O., Gruau, G., Dia, A., 2004. Impact of humate complexation on the
614 adsorption of REE onto Fe oxyhydroxide 277, 271–279. doi:10.1016/j.jcis.2004.04.007

615 Davranche, M., Pourret, O., Gruau, G., Dia, A., Bouhnik-Le Coz, M., 2005. Adsorption of REE
616 (III)-humate complexes onto MnO2: Experimental evidence for cerium anomaly and
617 lanthanide tetrad effect suppression. Geochemistry, Geophys. Geosystems 69, 4825–4835.
618 doi:10.1016/j.gca.2005.06.005

619 Desclaux, T., Lemonnier, H., Genthon, P., Soulard, B., Le Gendre, R., 2018. Suitability of a
620 lumped rainfall–runoff model for flashy tropical watersheds in New Caledonia. Hydrol. Sci.
621 J. 63, 1689–1706. doi:10.1080/02626667.2018.1523613

622 Dublet, G., Juillot, F., Morin, G., Fritsch, E., Noel, V., Brest, J., Brown, G.E., 2014. XAS
623 evidence for Ni sequestration by siderite in a lateritic Ni-deposit from New Caledonia. Am.
624 Mineral. doi:10.2138/am.2014.4625

Dubuc, A., Baker, R., Marchand, C., Waltham, N.J., Sheaves, M., 2019. Hypoxia in mangroves: Occurrence and impact on valuable tropical fish habitat. Biogeosciences 16, 3959–3976. doi:10.5194/bg-16-3959-2019

Elderfield, H., Greaves, M.J., 1982. The rare earth elements in seawater. Nature 296, 214–219. doi:10.1038/296214a0

FalconBridge NC, 2001. Projet Koniambo: Carte# 3. Etude environnementale de base. Carte syntese du milieu bio-physique et du milieu marin.

Garcia-Solsona, E., Jeandel, C., 2020. Balancing Rare Earth Element distributions in the Northwestern Mediterranean Sea. Chem. Geol. 532, 119372. doi:10.1016/j.chemgeo.2019.119372

Goldstein, S.J., Jacobsen, S.B., 1988. Rare earth elements in river waters. Earth Planet. Sci. Lett. 89, 35–47. doi:10.1016/0012-821X(88)90031-3

Hatje, V., Bruland, K.W., Flegal, A.R., 2016. Increases in Anthropogenic Gadolinium Anomalies and Rare Earth Element Concentrations in San Francisco Bay over a 20 Year Record. Environ. Sci. Technol. 50, 4159–4168. doi:10.1021/acs.est.5b04322

Hoyle, J., Elderfield, H., Gledhill, A., Greaves, M., 1983. The behavior of the rare earth elements during mixing of river and sea water. Geochim. Cosmochim. Acta 48, 13–149.

Kim, I., Kim, G., 2011. Large fluxes of rare earth elements through submarine groundwater discharge (SGD) from a volcanic island, Jeju, Korea. Mar. Chem. 127, 12–19. doi:10.1016/j.marchem.2011.07.006

Lawrence, M.G., Kamber, B.S., 2006. The behaviour of the rare earth elements during estuarine mixing-revisited. Mar. Chem. 100, 147–161. doi:10.1016/j.marchem.2005.11.007

Lee, K., Grundstein, A.J., Wenner, D.B., Choi, M., Woo, N., Lee, D., 2003. Climatic controls on the stable isotopic composition of precipitation in Northeast Asia. Clim. Res. 23, 137–148.

Lillie, A.R., Brothers, R.N., 1970. The geology of New Caledonia. New Zeal. J. Geol. Geophys. 13, 145–183. doi:10.1080/00288306.1970.10428210

651 Ma, L., Dang, D.H., Wang, Wei, Evans, R.D., Wang, Wen-xiong, 2019. Rare earth elements in
652 the Pearl River Delta of China: Potential impacts of the REE industry on water, suspended
653 particles and oysters. Environ. Pollut. 244, 190–201. doi:10.1016/j.envpol.2018.10.015

654 Marchand, C., Fernandez, J.M., Moreton, B., Landi, L., Lallier-Vergès, E., Baltzer, F., 2012. The
655 partitioning of transitional metals (Fe, Mn, Ni, Cr) in mangrove sediments downstream of a
656 ferralitized ultramafic watershed (New Caledonia). Chem. Geol.
657 doi:10.1016/j.chemgeo.2012.01.018

658 Marsac, R., Davranche, M., Gruau, G., Dia, A., 2010. Metal loading effect on rare earth element
659 binding to humic acid: Experimental and modelling evidence. Geochim. Cosmochim. Acta
660 74, 1749–1761. doi:10.1016/j.gca.2009.12.006

661 McLennan, S.M., 2001. Relationships between the trace element composition of sedimentary
662 rocks and upper continental crust. Geochemistry, Geophys. Geosystems 2, 2000GC000109.
663 doi:10.1038/scientificamerican0983-130

664 Merrot, P., Juillot, F., Noël, V., Lefebvre, P., Brest, J., Menguy, N., Guigner, J.M., Blondeau, M.,
665 Viollier, E., Fernandez, J.M., Moreton, B., Bargar, J.R., Morin, G., 2019. Nickel and iron
666 partitioning between clay minerals, Fe-oxides and Fe-sulfides in lagoon sediments from
667 New Caledonia. Sci. Total Environ. doi:10.1016/j.scitotenv.2019.06.274

668 Munksgaard, N.C., Wurster, C.M., Bass, A., Zagorskis, I., Bird, M.I., 2012. First continuous
669 shipboard δ 18O and δD measurements in sea water by diffusion sampling-cavity ring-down
670 spectrometry. Environ. Chem. Lett. 10, 301–307. doi:10.1007/s10311-012-0371-5

671 Noël, V., Marchand, C., Juillot, F., Ona-Nguema, G., Viollier, E., Marakovic, G., Olivi, L.,
672 Delbes, L., Gelebart, F., Morin, G., 2014. EXAFS analysis of iron cycling in mangrove
673 sediments downstream a lateritized ultramafic watershed (Vavouto Bay, New Caledonia).
674 Geochim. Cosmochim. Acta 136, 211–228. doi:10.1016/j.gca.2014.03.019

675 Nozaki, Y., Lerche, D., Alibo, D.S., Snidvongs, A., 2000. The estuarine geochemistry of rare
676 earth elements and indium in the Chao Phraya River, Thailand. Geochim. Cosmochim. Acta
677 64, 3983–3994. doi:10.1016/S0016-7037(00)00473-7

678 Och, L.M., Muller, B., Wichser, A., Ulrich, A., Vologina, E.G., Sturm, M., 2014. Rare earth
679 elements in the sediments of Lake Baikal. Chem. Geol. 376, 61–75.
680 doi:10.1016/j.chemgeo.2014.03.018

681 Paffrath, R., Pahnke, K., Behrens, M., Reckhardt, A., Ehlert, C., Schnetger, B., Brumsack, H.-J.,
682 2020. Rare Earth Element Behavior in a Sandy Subterranean Estuary of the Southern North
683 Sea. Front. Mar. Sci. 7, 424. doi:10.3389/fmars.2020.00424

684 Piper, D.Z., Bau, M., 2013. Normalized Rare Earth Elements in Water , Sediments , and Wine :
685 Identifying Sources and Environmental Redox Conditions. Am. J. Anal. Chem. 4, 69–83.
686 doi:10.4236/ajac.2013.410A1009

687 Planavsky, N., Bekker, A., Rouxel, O.J., Kamber, B., Hofmann, A., Knudsen, A., Lyons, T.W.,
688 2010. Rare Earth Element and yttrium compositions of Archean and Paleoproterozoic Fe
689 formations revisited: New perspectives on the significance and mechanisms of deposition.
690 Geochim. Cosmochim. Acta 74, 6387–6405. doi:10.1016/j.gca.2010.07.021

691 Pourret, O., Davranche, M., 2013. Rare earth element sorption onto hydrous manganese oxide: A
692 modeling study. J. Colloid Interface Sci. 395, 18–23. doi:10.1016/j.jcis.2012.11.054

693 Pourret, O., Tuduri, J., 2017. Continental shelves as potential resource of rare earth elements. Sci.
694 Rep. 7, 1–6. doi:10.1038/s41598-017-06380-z

695 Rigaud, S., Radakovitch, O., Couture, R.-M., Deflandre, B., Cossa, D., Garnier, C., Garnier, J.-
696 M., 2013. Mobility and fluxes of trace elements and nutrients at the sediment–water
697 interface of a lagoon under contrasting water column oxygenation conditions. Appl.
698 Geochemistry 31, 35–51. doi:10.1016/j.apgeochem.2012.12.003

699 Rohling, E.J., 2007. Progress in paleosalinity: Overview and presentation of a new approach.
700 Paleoceanography. doi:10.1029/2007PA001437

701 Rousseau, T.C.C., Sonke, J.E., Chmeleff, J., Van Beek, P., Souhaut, M., Boaventura, G., Seyler,
702 P., Jeandel, C., 2015. Rapid neodymium release to marine waters from lithogenic sediments
703 in the Amazon estuary. Nat. Commun. 6. doi:10.1038/ncomms8592

704 Rudnick, R., Gao, S., 2003. Composition of the continental crust, in: Turekian, K.K., Holland,

H.D. (Eds.), Treatise on Geochemistry. Elsevier Ltd, pp. 1–64.

Sholkovitz, E., Szymczak, R., 2000. The estuarine chemistry of rare earth elements: Comparison of the Amazon, Fly, Sepik and the Gulf of Papua systems. Earth Planet. Sci. Lett. 179, 299–309. doi:10.1016/S0012-821X(00)00112-6

Sholkovitz, E.R., 1995. The aquatic chemistry of rare earth elements in rivers and estuaries. Aquat. Geochemistry 1, 1–34. doi:10.1007/BF01025229

Spalding, M., 2010. World Atlas of Mangroves, World Atlas of Mangroves. doi:10.4324/9781849776608

Tachikawa, K., Athias, V., Jeandel, C., 2003. Neodymium budget in the modern ocean and paleo-oceanographic implications. J. Geophys. Res. Ocean. 108, 1–13. doi:10.1029/1999jc000285

Taureau, F., Robin, M., Proisy, C., Fromard, F., Imbert, D., Debaine, F., 2019. Mapping the mangrove forest canopy using spectral unmixing of very high spatial resolution satellite images. Remote Sens. 11. doi:10.3390/rs11030367

Tepe, N., Romero, M., Bau, M., 2014. High-technology metals as emerging contaminants: Strong increase of anthropogenic gadolinium levels in tap water of Berlin, Germany, from 2009 to 2012. Appl. Geochemistry 45, 191–197. doi:10.1016/j.apgeochem.2014.04.006

Terry, J.P., Wotling, G., 2011. Rain-shadow hydrology: Influences on river flows and flood magnitudes across the central massif divide of La Grande Terre Island, New Caledonia. J. Hydrol. 404, 77–86. doi:10.1016/j.jhydrol.2011.04.022

Wallace, M.W., Hood, A., Shuster, A., Greig, A., Planavsky, N.J., Reed, C.P., 2017. Oxygenation history of the Neoproterozoic to early Phanerozoic and the rise of land plants. Earth Planet. Sci. Lett. 466, 12–19. doi:10.1016/j.epsl.2017.02.046

Wolfe, B.B., Karst-Riddoch, T.L., Hall, R., Edwards, T., English, M., Palmini, R., Mcgowan, S., Leavitt, P., Vardy, S., 2007. Classification of hydrological regimes of northern floodplain basins (Peace–Athabasca Delta, Canada) from analysis of stable isotopes (d18O, d2H) and water chemistry. Hydrol. Process. 21, 151–168. doi:10.1002/hyp.6229 Classification

Yeghicheyan, D., Aubert, D., Bouhnik-Le Coz, M., Chmeleff, J., Delpoux, S., Djouraev, I.,

Granier, G., Lacan, F., Piro, J.L., Rousseau, T., Cloquet, C., Marquet, A., Menniti, C., Pradoux, C., Freydier, R., Vieira da Silva-Filho, E., Suchorski, K., 2019. A New Interlaboratory Characterisation of Silicon, Rare Earth Elements and Twenty-Two Other Trace Element Concentrations in the Natural River Water Certified Reference Material SLRS-6 (NRC-CNRC). Geostand. Geoanalytical Res. 43, 475–496. doi:10.1111/ggr.12268

(2) Auer, G.; Reuter, M.; Hauzenberger, C. A.; Piller, W. E. The Impact of Transport Processes on Rare Earth Element Patterns in Marine Authigenic and Biogenic Phosphates. *Geochim. Cosmochim. Acta* **2017**, *203*, 140–156. https://doi.org/10.1016/j.gca.2017.01.001.

(3) Wallace, M. W.; Hood, A.; Shuster, A.; Greig, A.; Planavsky, N. J.; Reed, C. P. Oxygenation History of the Neoproterozoic to Early Phanerozoic and the Rise of Land Plants. *Earth Planet. Sci. Lett.* **2017**, *466*, 12–19. https://doi.org/10.1016/j.epsl.2017.02.046.

(4) Planavsky, N.; Bekker, A.; Rouxel, O. J.; Kamber, B.; Hofmann, A.; Knudsen, A.; Lyons, T. W. Rare Earth Element and Yttrium Compositions of Archean and Paleoproterozoic Fe Formations Revisited: New Perspectives on the Significance and Mechanisms of Deposition. *Geochim. Cosmochim. Acta* **2010**, *74* (22), 6387–6405. https://doi.org/10.1016/j.gca.2010.07.021.

(5) Tepe, N.; Romero, M.; Bau, M. High-Technology Metals as Emerging Contaminants: Strong Increase of Anthropogenic Gadolinium Levels in Tap Water of Berlin, Germany, from 2009 to 2012. *Appl. Geochemistry* **2014**, *45*, 191–197. https://doi.org/10.1016/j.apgeochem.2014.04.006.

(6) Dang, D. H.; Zhang, Z. Hazardous Motherboards: Evolution of Electronic Technologies and Transition in Metals Contamination. *Environ. Pollut.* **2021**, *268*, 115731.

(7) Ma, L.; Dang, D. H.; Wang, W.; Evans, R. D.; Wang, W. Rare Earth Elements in the Pearl River Delta of China: Potential Impacts of the REE Industry on Water, Suspended Particles and Oysters. *Environ. Pollut.* **2019**, *244*, 190–201.

https://doi.org/10.1016/j.envpol.2018.10.015.

(8) Sholkovitz, E. R. The Aquatic Chemistry of Rare Earth Elements in Rivers and Estuaries. *Aquat. Geochemistry* **1995**, *1* (1), 1–34. https://doi.org/10.1007/BF01025229.

(9) Sholkovitz, E.; Szymczak, R. The Estuarine Chemistry of Rare Earth Elements: Comparison of the Amazon, Fly, Sepik and the Gulf of Papua Systems. *Earth Planet. Sci. Lett.* **2000**, *179* (2), 299–309. https://doi.org/10.1016/S0012-821X(00)00112-6.

(10) Nozaki, Y.; Lerche, D.; Alibo, D. S.; Snidvongs, A. The Estuarine Geochemistry of Rare Earth Elements and Indium in the Chao Phraya River, Thailand. *Geochim. Cosmochim. Acta* **2000**, *64* (23), 3983–3994. https://doi.org/10.1016/S0016-7037(00)00473-7.

(11) Pourret, O.; Tuduri, J. Continental Shelves as Potential Resource of Rare Earth Elements. *Sci. Rep.* **2017**, *7* (1), 1–6. https://doi.org/10.1038/s41598-017-06380-z.

(12) Elderfield, H.; Greaves, M. J. The Rare Earth Elements in Seawater. *Nature* **1982**, *296* (5854), 214–219. https://doi.org/10.1038/296214a0.

(13) Lawrence, M. G.; Kamber, B. S. The Behaviour of the Rare Earth Elements during Estuarine Mixing-Revisited. *Mar. Chem.* **2006**, *100* (1–2), 147–161. https://doi.org/10.1016/j.marchem.2005.11.007.

(14) Hoyle, J.; Elderfield, H.; Gledhill, A.; Greaves, M. The Behavior of the Rare Earth Elements during Mixing of River and Sea Water. *Geochim. Cosmochim. Acta* **1983**, *48* (0016–7037), 13–149.

(15) Bau, M.; Moller, P.; Dulski, P. Yttrium and Lanthanides in Eastern Mediterranean Seawater and Their Fractionation during Redox-Cycling. *Mar. Chem.* **1997**, *56*, 123–131.

(16) Spalding, M. *World Atlas of Mangroves*; 2010. https://doi.org/10.4324/9781849776608.

(17) Dubuc, A.; Baker, R.; Marchand, C.; Waltham, N. J.; Sheaves, M. Hypoxia in Mangroves: Occurrence and Impact on Valuable Tropical Fish Habitat. *Biogeosciences* **2019**, *16* (20), 3959–3976. https://doi.org/10.5194/bg-16-3959-2019.

(18) Marchand, C.; Fernandez, J. M.; Moreton, B.; Landi, L.; Lallier-Vergès, E.; Baltzer, F.

The Partitioning of Transitional Metals (Fe, Mn, Ni, Cr) in Mangrove Sediments Downstream of a Ferralitized Ultramafic Watershed (New Caledonia). *Chem. Geol.* **2012**. https://doi.org/10.1016/j.chemgeo.2012.01.018.

(19) Lillie, A. R.; Brothers, R. N. The Geology of New Caledonia. *New Zeal. J. Geol. Geophys.* **1970**, *13* (1), 145–183. https://doi.org/10.1080/00288306.1970.10428210.

(20) Dublet, G.; Juillot, F.; Morin, G.; Fritsch, E.; Noel, V.; Brest, J.; Brown, G. E. XAS Evidence for Ni Sequestration by Siderite in a Lateritic Ni-Deposit from New Caledonia. *Am. Mineral.* **2014**. https://doi.org/10.2138/am.2014.4625.

(21) Noël, V.; Marchand, C.; Juillot, F.; Ona-Nguema, G.; Viollier, E.; Marakovic, G.; Olivi, L.; Delbes, L.; Gelebart, F.; Morin, G. EXAFS Analysis of Iron Cycling in Mangrove Sediments Downstream a Lateritized Ultramafic Watershed (Vavouto Bay, New Caledonia). *Geochim. Cosmochim. Acta* **2014**, *136*, 211–228. https://doi.org/10.1016/j.gca.2014.03.019.

(22) Fritsch, E.; Juillot, F.; Dublet, G.; Fonteneau, L.; Fandeur, D.; Martin, E.; Caner, L.; Auzende, A.-L.; Grauby, O.; Beaufort, D. An Alternative Model for the Formation of Hydrous Mg/Ni Layer Silicates ('deweylite'/'garnierite') in Faulted Peridotites of New Caledonia: I. Texture and Mineralogy of a Paragenetic Succession of Silicate Infillings. *Eur. J. Mineral.* **2016**, *28* (2), 295–311. https://doi.org/10.1127/ejm/2015/0027-2503.

(23) Yeghicheyan, D.; Aubert, D.; Bouhnik-Le Coz, M.; Chmeleff, J.; Delpoux, S.; Djouraev, I.; Granier, G.; Lacan, F.; Piro, J. L.; Rousseau, T.; et al. A New Interlaboratory Characterisation of Silicon, Rare Earth Elements and Twenty-Two Other Trace Element Concentrations in the Natural River Water Certified Reference Material SLRS-6 (NRC-CNRC). *Geostand. Geoanalytical Res.* **2019**, *43* (3), 475–496. https://doi.org/10.1111/ggr.12268.

(24) Piper, D. Z.; Bau, M. Normalized Rare Earth Elements in Water , Sediments , and Wine : Identifying Sources and Environmental Redox Conditions. *Am. J. Anal. Chem.* **2013**, *4*, 69–83. https://doi.org/10.4236/ajac.2013.410A1009.

(25) McLennan, S. M. Relationships between the Trace Element Composition of Sedimentary

Rocks and Upper Continental Crust. *Geochemistry, Geophys. Geosystems* **2001**, *2*, 2000GC000109. https://doi.org/10.1038/scientificamerican0983-130.

(26) Goldstein, S. J.; Jacobsen, S. B. Rare Earth Elements in River Waters. *Earth Planet. Sci. Lett.* **1988**, *89* (1), 35–47. https://doi.org/10.1016/0012-821X(88)90031-3.

(27) Hatje, V.; Bruland, K. W.; Flegal, A. R. Increases in Anthropogenic Gadolinium Anomalies and Rare Earth Element Concentrations in San Francisco Bay over a 20 Year Record. *Environ. Sci. Technol.* **2016**, *50* (8), 4159–4168. https://doi.org/10.1021/acs.est.5b04322.

(28) Conroy, J. L.; Cobb, K. M.; Lynch-Stieglitz, J.; Polissar, P. J. Constraints on the Salinity-Oxygen Isotope Relationship in the Central Tropical Pacific Ocean. *Mar. Chem.* **2014**, *161*, 26–33. https://doi.org/10.1016/j.marchem.2014.02.001.

(29) Rohling, E. J. Progress in Paleosalinity: Overview and Presentation of a New Approach. *Paleoceanography*. 2007. https://doi.org/10.1029/2007PA001437.

(30) Wolfe, B. B.; Karst-Riddoch, T. L.; Hall, R.; Edwards, T.; English, M.; Palmini, R.; Mcgowan, S.; Leavitt, P.; Vardy, S. Classification of Hydrological Regimes of Northern Floodplain Basins (Peace–Athabasca Delta, Canada) from Analysis of Stable Isotopes (D18O, D2H) and Water Chemistry. *Hydrol. Process.* **2007**, *21*, 151–168. https://doi.org/10.1002/hyp.6229 Classification.

(31) Dansgaard, W. Stable Isotopes in Precipitation. *Tellus* **1964**. https://doi.org/10.3402/tellusa.v16i4.8993.

(32) Lee, K.; Grundstein, A. J.; Wenner, D. B.; Choi, M.; Woo, N.; Lee, D. Climatic Controls on the Stable Isotopic Composition of Precipitation in Northeast Asia. *Clim. Res.* **2003**, *23*, 137–148.

(33) Munksgaard, N. C.; Wurster, C. M.; Bass, A.; Zagorskis, I.; Bird, M. I. First Continuous Shipboard δ 18O and ΔD Measurements in Sea Water by Diffusion Sampling-Cavity Ring-down Spectrometry. *Environ. Chem. Lett.* **2012**, *10* (3), 301–307. https://doi.org/10.1007/s10311-012-0371-5.

(34) Conroy, J. L.; Thompson, D. M.; Cobb, K. M.; Noone, D.; Rea, S.; Legrande, A. N. Spatiotemporal Variability in the Δ18O-Salinity Relationship of Seawater across the Tropical Pacific Ocean. *Paleoceanography* **2017**, *32* (5), 484–497. https://doi.org/10.1002/2016PA003073.

(35) Censi, P.; Mazzola, S.; Sprovieri, M.; Bonanno, A.; Patti, B.; Punturo, R.; Spoto, S. E.; Saiano, F.; Alonzo, G. Rare Earth Elements Distribution in Seawater and Suspended Particulate of the Central Mediterranean Sea. *Chem. Ecol.* **2004**, *20* (5), 323–343. https://doi.org/10.1080/02757540410001727954.

(36) Och, L. M.; Muller, B.; Wichser, A.; Ulrich, A.; Vologina, E. G.; Sturm, M. Rare Earth Elements in the Sediments of Lake Baikal. *Chem. Geol.* **2014**, *376*, 61–75. https://doi.org/10.1016/j.chemgeo.2014.03.018.

(37) Paffrath, R.; Pahnke, K.; Behrens, M.; Reckhardt, A.; Ehlert, C.; Schnetger, B.; Brumsack, H.-J. Rare Earth Element Behavior in a Sandy Subterranean Estuary of the Southern North Sea. *Front. Mar. Sci.* **2020**, *7*, 424. https://doi.org/10.3389/fmars.2020.00424.

(38) Dang, D. H.; Layglon, N.; Ferretto, N.; Omanović, D.; Mullot, J.-U.; Lenoble, V.; Mounier, S.; Garnier, C. Kinetic Processes of Copper and Lead Remobilization during Sediment Resuspension of Marine Polluted Sediments. *Sci. Total Environ.* **2020**, *698*, 134120.

(39) Garcia-Solsona, E.; Jeandel, C. Balancing Rare Earth Element Distributions in the Northwestern Mediterranean Sea. *Chem. Geol.* **2020**, *532* (June 2019), 119372. https://doi.org/10.1016/j.chemgeo.2019.119372.

(40) Marsac, R.; Davranche, M.; Gruau, G.; Dia, A. Metal Loading Effect on Rare Earth Element Binding to Humic Acid: Experimental and Modelling Evidence. *Geochim. Cosmochim. Acta* **2010**, *74* (6), 1749–1761. https://doi.org/10.1016/j.gca.2009.12.006.

(41) Davranche, M.; Pourret, O.; Gruau, G.; Dia, A. Impact of Humate Complexation on the Adsorption of REE onto Fe Oxyhydroxide. **2004**, *277*, 271–279. https://doi.org/10.1016/j.jcis.2004.04.007.

(42) Pourret, O.; Davranche, M. Rare Earth Element Sorption onto Hydrous Manganese Oxide: A Modeling Study. *J. Colloid Interface Sci.* **2013**, *395* (1), 18–23. https://doi.org/10.1016/j.jcis.2012.11.054.

(43) Rudnick, R.; Gao, S. Composition of the Continental Crust. In *Treatise on geochemistry*; Turekian, K. K., Holland, H. D., Eds.; Elsevier Ltd, 2003; Vol. 1, pp 1–64.

(44) Davranche, M.; Pourret, O.; Gruau, G.; Dia, A.; Bouhnik-Le Coz, M. Adsorption of REE (III)-Humate Complexes onto MnO2: Experimental Evidence for Cerium Anomaly and Lanthanide Tetrad Effect Suppression. *Geochemistry, Geophys. Geosystems* **2005**, *69* (20), 4825–4835. https://doi.org/10.1016/j.gca.2005.06.005.

(45) Byrne, R. H.; Lee, J. H. Comparative Yttrium and Rare Earth Element Chemistries in Seawater. *Mar. Chem.* **1993**. https://doi.org/10.1016/0304-4203(93)90197-V.

(46) Bau, M.; Dulski, P.; Moller, P. Yttrium and Holmium in South Pacific Seawater : Vertical Distribution and Possible Fractionation Mechanisms. *Chemie der Erde - Geochemistrymie der Erde* **1995**, *55*, 1–15.

(47) Dang, D. H.; Lenoble, V.; Durrieu, G.; Omanović, D.; Mullot, J.-U.; Mounier, S.; Garnier, C. Seasonal Variations of Coastal Sedimentary Trace Metals Cycling: Insight on the Effect of Manganese and Iron (Oxy)Hydroxides, Sulphide and Organic Matter. *Mar. Pollut. Bull.* **2015**, *92*, 113–124. https://doi.org/10.1016/j.marpolbul.2014.12.048.

(48) Arsouze, T.; Dutay, J.-C.; Lacan, F.; Jeandel, C. Reconstructing the Nd Oceanic Cycle Using a Coupled Dynamical – Biogeochemical Model. *Biogeosciences Discuss.* **2009**, *6* (3), 5549–5588. https://doi.org/10.5194/bgd-6-5549-2009.

(49) Tachikawa, K.; Athias, V.; Jeandel, C. Neodymium Budget in the Modern Ocean and Paleo-Oceanographic Implications. *J. Geophys. Res. Ocean.* **2003**, *108* (8), 1–13. https://doi.org/10.1029/1999jc000285.

(50) DAVAR Service de l'eau. *Synthèse Ressource En Eau*; 2019; Vol. Décembre.

(51) Taureau, F.; Robin, M.; Proisy, C.; Fromard, F.; Imbert, D.; Debaine, F. Mapping the Mangrove Forest Canopy Using Spectral Unmixing of Very High Spatial Resolution

Satellite Images. *Remote Sens.* **2019**, *11* (3). https://doi.org/10.3390/rs11030367.

(52) FalconBridge NC. *Projet Koniambo: Carte# 3. Étude Environnementale de Base. Carte Synthèse Du Milieu Bio-Physique et Du Milieu Marin*; 2001.

(53) Rousseau, T. C. C.; Sonke, J. E.; Chmeleff, J.; Van Beek, P.; Souhaut, M.; Boaventura, G.; Seyler, P.; Jeandel, C. Rapid Neodymium Release to Marine Waters from Lithogenic Sediments in the Amazon Estuary. *Nat. Commun.* **2015**, *6* (May). https://doi.org/10.1038/ncomms8592.

(54) Kim, I.; Kim, G. Large Fluxes of Rare Earth Elements through Submarine Groundwater Discharge (SGD) from a Volcanic Island, Jeju, Korea. *Mar. Chem.* **2011**, *127* (1–4), 12–19. https://doi.org/10.1016/j.marchem.2011.07.006.

(55) Dang, D. H.; Lenoble, V.; Durrieu, G.; Mullot, J.-U.; Mounier, S.; Garnier, C. Sedimentary Dynamics of Coastal Organic Matter: An Assessment of the Porewater Size/Reactivity Model by Spectroscopic Techniques. *Estuar. Coast. Shelf Sci.* **2014**, *151*, 100–111. https://doi.org/10.1016/j.ecss.2014.10.002.

(56) Rigaud, S.; Radakovitch, O.; Couture, R.-M.; Deflandre, B.; Cossa, D.; Garnier, C.; Garnier, J.-M. Mobility and Fluxes of Trace Elements and Nutrients at the Sediment–Water Interface of a Lagoon under Contrasting Water Column Oxygenation Conditions. *Appl. Geochemistry* **2013**, *31*, 35–51. https://doi.org/10.1016/j.apgeochem.2012.12.003.

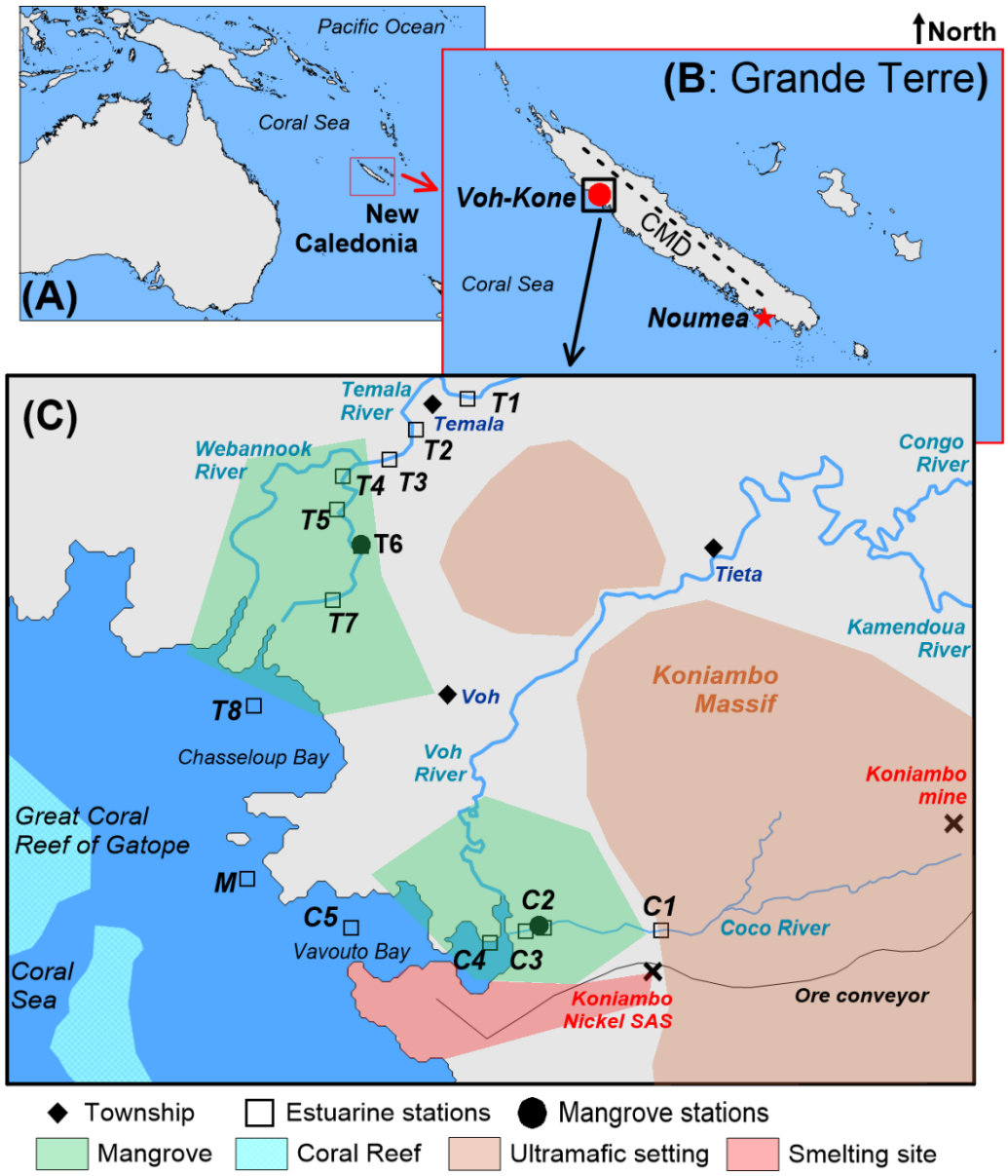

Figure 1: Map of New Caledonia (A), the two regions under investigation: Voh-Kone region (red circle) and four rivers in the Southeast of Grande Terre (red star), around Noumea (B), and a zoom into the Voh-Kone region with sampling locations (C). The position of the CMD (Central Massive Divide) in B is approximative. The southwestern basins of the CMD are considered leeward while the northeastern are windward. See text for more details on the study sites.

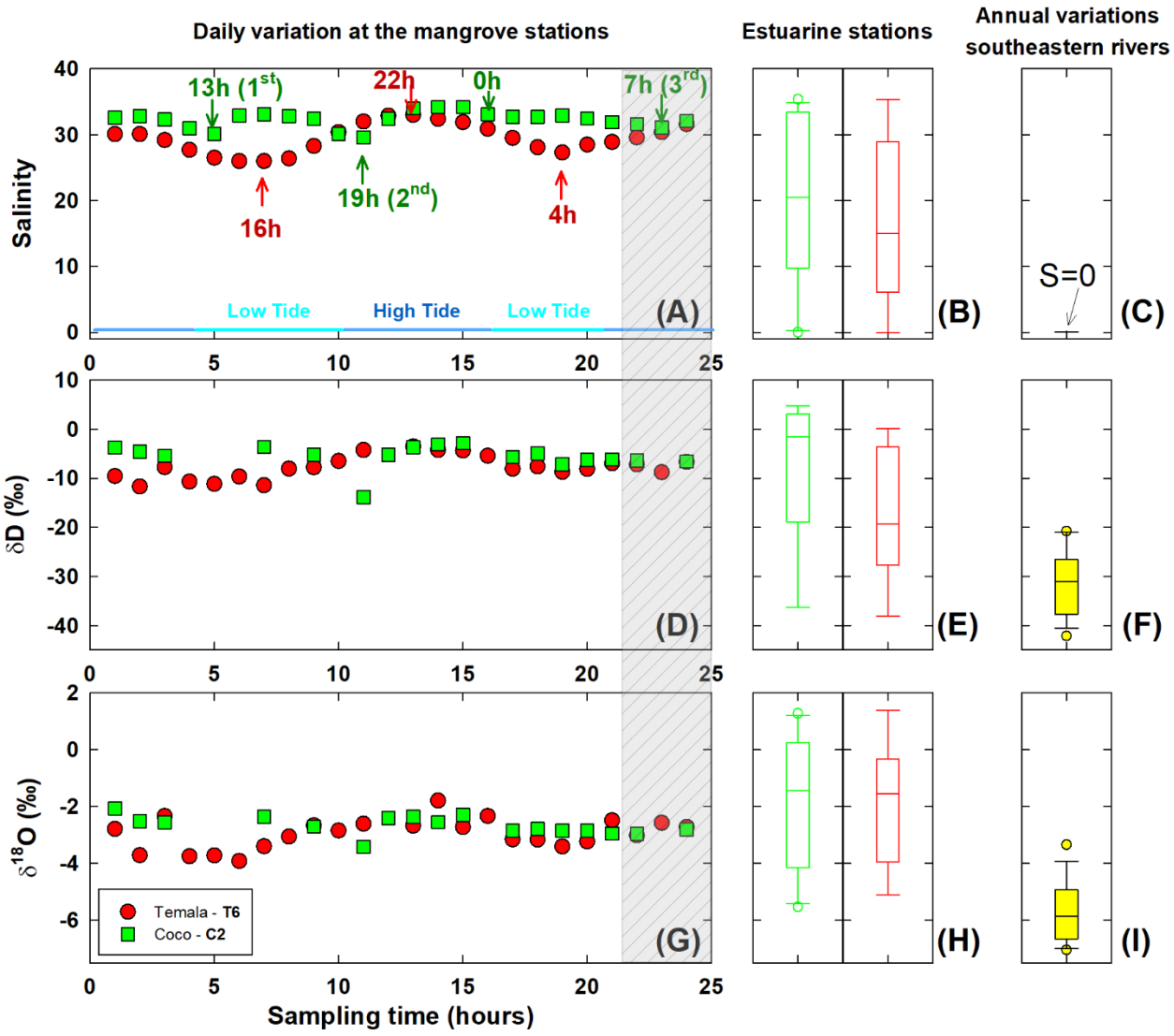

Figure 2: Variations in salinity, δD and $\delta^{18}O$ in waters collected from the Temala (red symbols) and Coco (green symbols) Rivers of the Voh-Kone regions and four rivers of the Southeast (yellow boxes). Left panels (A, D, G) show the daily variations recorded within 24 hours in the mangrove forest (stations T6 and C2). The arabic numbers (1^{st}, 2^{nd}, 3^{rd}) indicates the three events where freshwaters were discharged from the Coco river toward the lagoon. The greyed zone shows the last samples collected of the 24-hour series during high tide where all physical-chemical properties and stable water isotopes of the two rivers overlaps. Those data are excluded from the δD-salinity regresssion of Temala River as justified in text. Middle box plots (B, E, H) summarize the spatial variations of Temala and Coco estuaries. The right box plots (C, F, I) show the annual variations of the four rivers in the Southeast of New Caledonia. For all box plots, the horinzonal lines in boxes show median values while box boundaries indicate the 25^{th} and 75^{th} percentiles. The whiskers demark the 10^{th} and 90^{th} percentiles and scatters are values of the 5^{th} and 95^{th} percentile range.

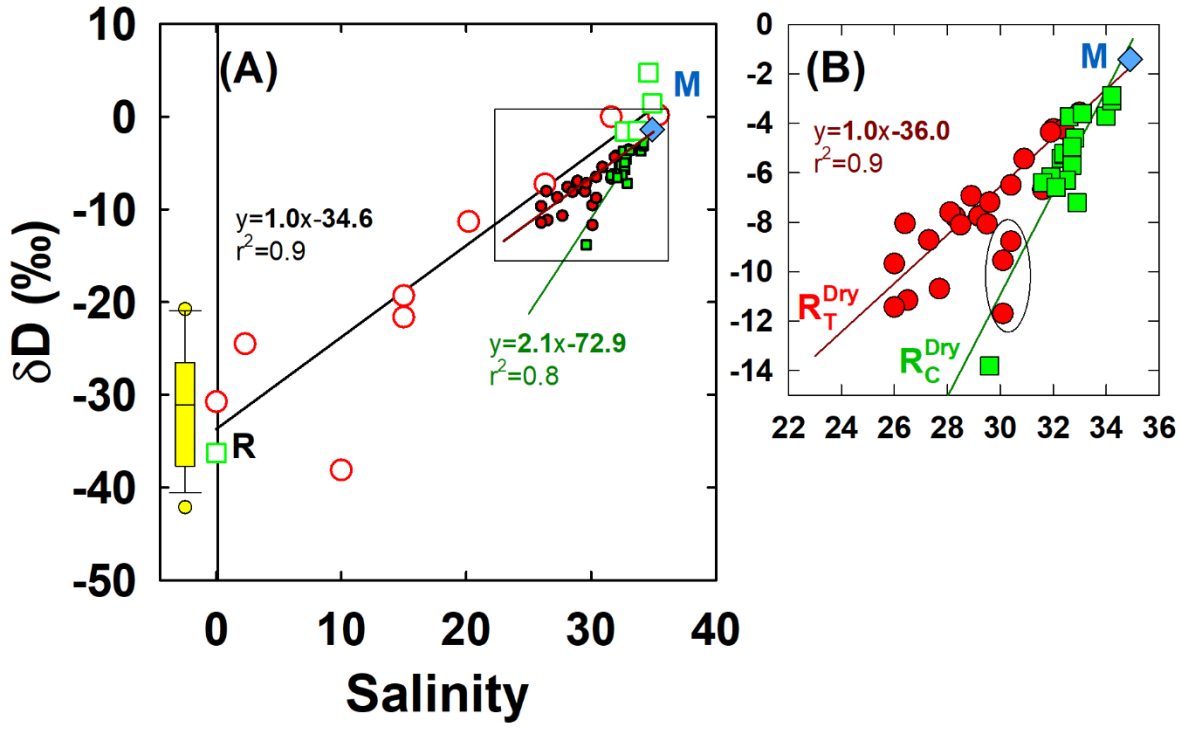

Figure 3: (A) δD-Salinity biplots of all waters collected from the Coco (green symbols), Temala (red symbols) and the box plot of four rivers in the Southeast (yellow, salinity = 0, see legend of Figure 2 for more details). Samples collected in the mangrove forests (full red and green symbols), across the estuaries (open red and green symbols) and the marine endmember (blue diamond) are also shown. A zoom in the Coco and Temala system during dry season is provided in panel (B). Their respective regression lines are shown in red (Temala) and green (green) while the black regression line represents all samples from Temala and Coco estuaries. The regression for Temala River excludes the data (encircled in B) that are observed on the Coco River regression lines. See text for justification.

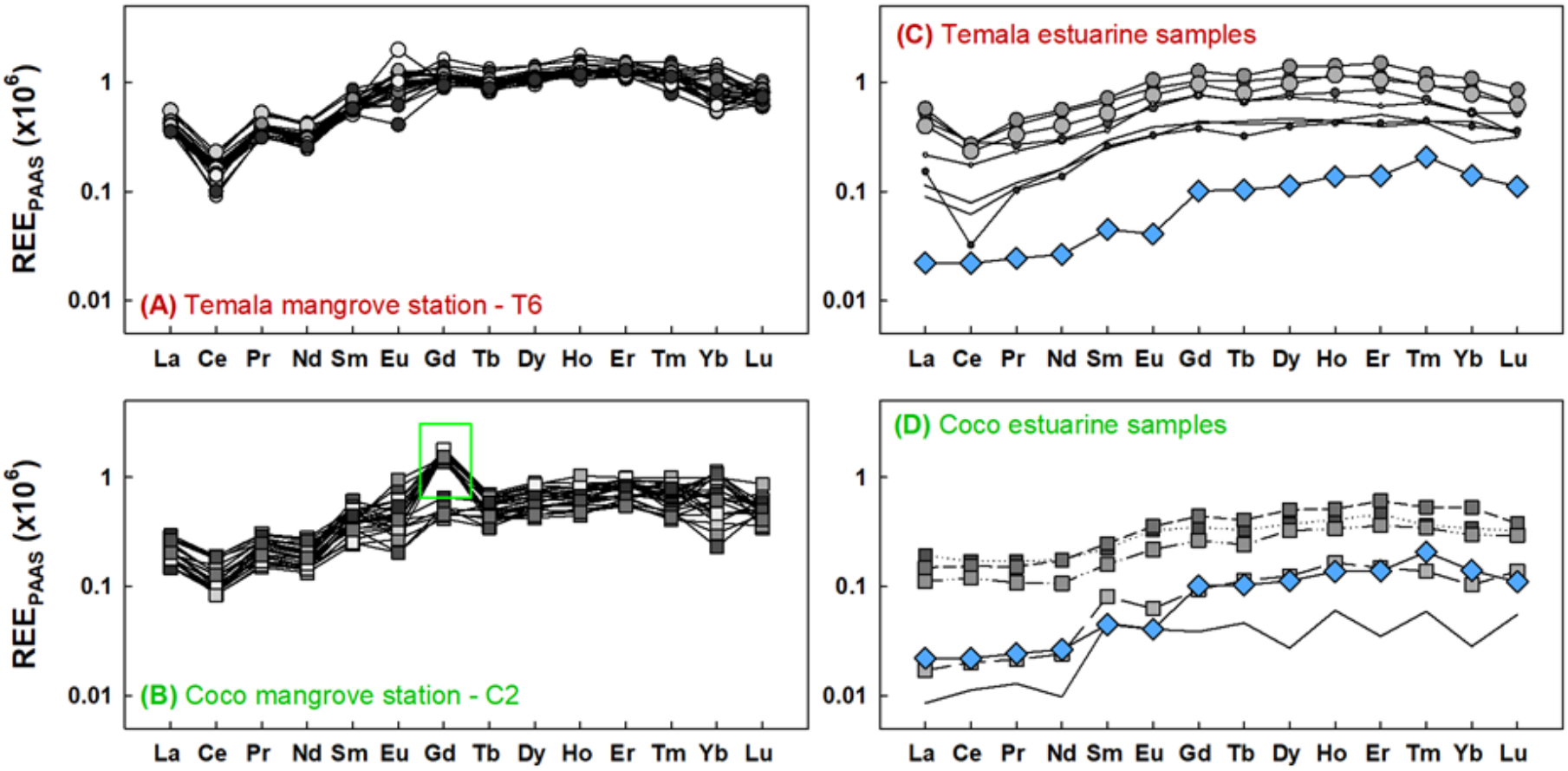

Figure 4: Rare earth element patterns in the waters of the mangrove stations (T6 and C2) at Temala (A) and Coco (B), and across the estuarine mixing of Temala (C) and Coco (D). The blue diamonds show the REE patterns in the marine endmember. The gray intensity of the symbols in panels A and B is associated with the 24-h time-series (black symbols corresponding to the first sampling). The symbol size in panels C and D reflect the salinity (small symbols reflecting freshwater). The green rectangle in B demarks Gd anomalies observed in Coco River water.

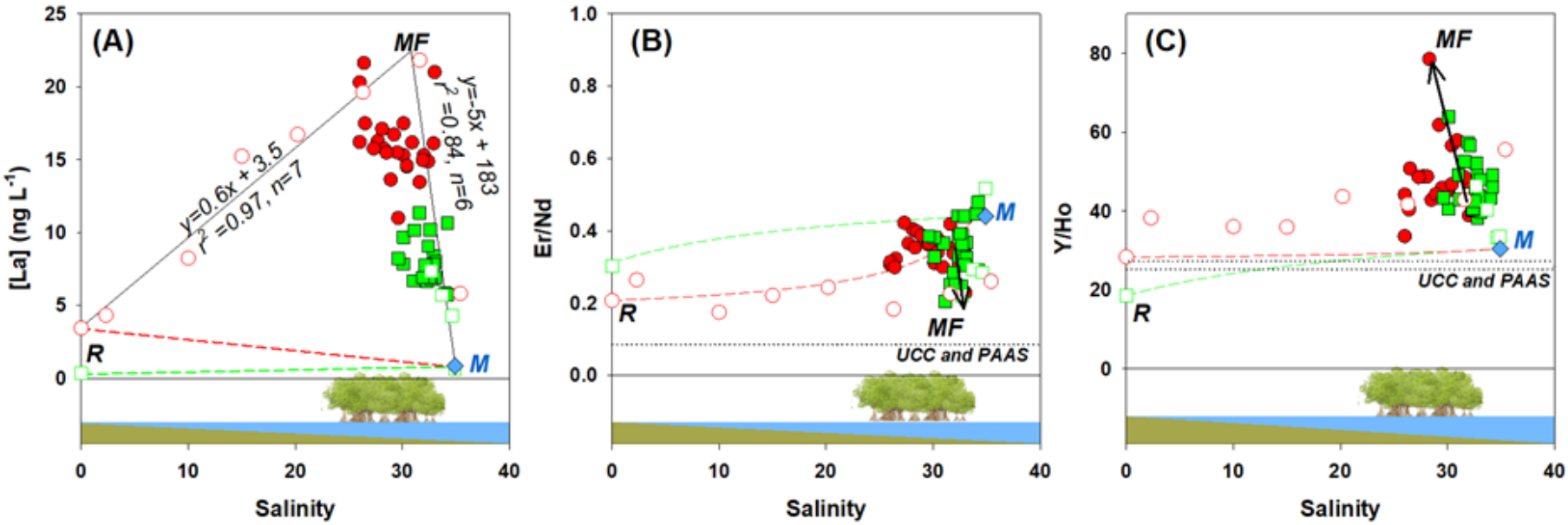

Figure 5: Variations of La concentrations (A), Er/Nd (B) and Y/Ho (C) ratios as the function of salinity at Temala (red symbols) and Coco (green symbols). Samples in the mangrove forests are shown by full symbols while estuarine samples are presented as open symbols. The blue diamond symbols represent the marine endmember. The horizontal dotted lines show the values in the Upper Continental Crust (UCC) and PAAS shale. The dotted green and red lines are conservative mixing line for Coco and Temala estuaries, respectively.

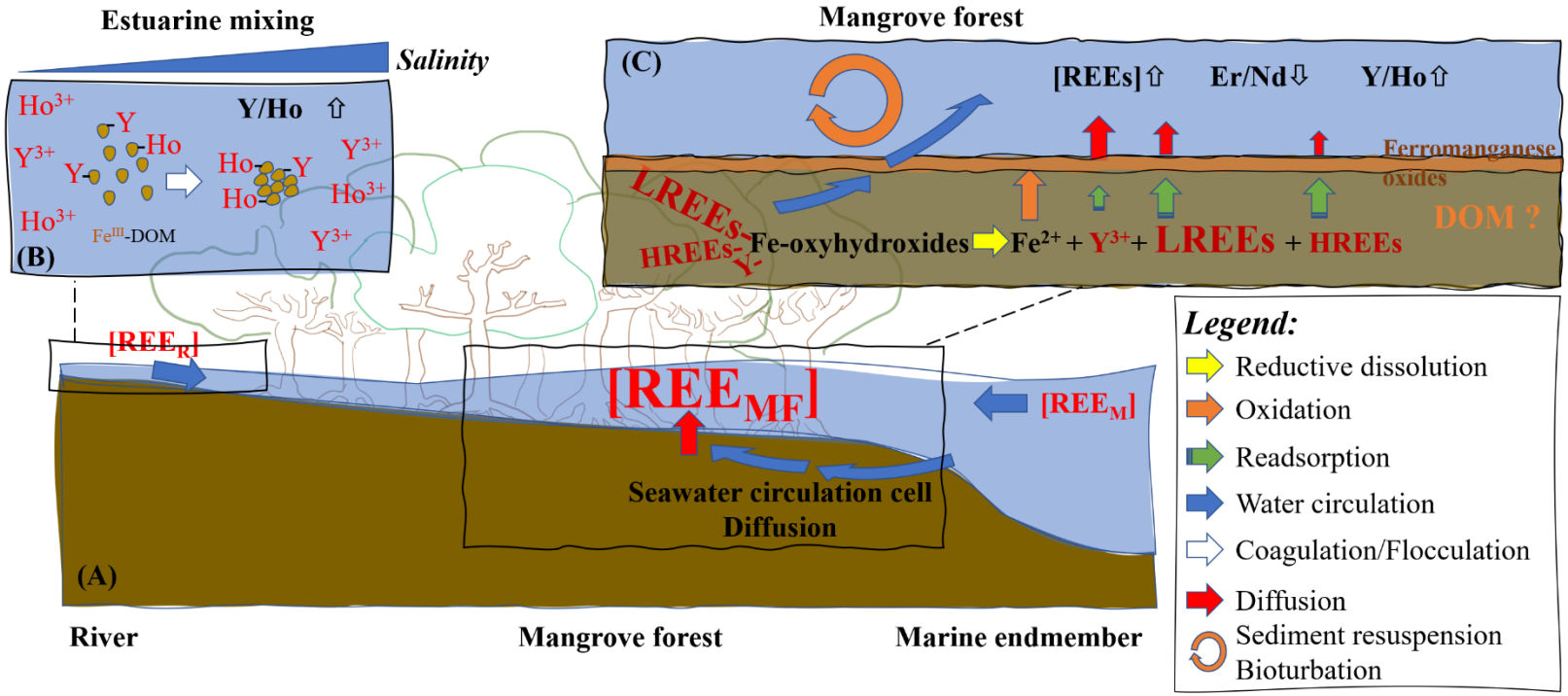

Figure 6: Schematic represention of the REE cycle in tropical mangrove-dominated estuaries (A). Panels (B) and (C) provide a zoom into the mechanisms occuring across the estuarine mixing and within the mangrove forest, respectively. In (B), the flocculation of either dissolved organic Fe^{III} complexes (Fe^{III}-DOM) or colloidal particles is presented.

Table 1: Variations in the physical-chemical properties of water collected over a 24-hour cycle in the dry season in the Temala (T6) and Coco (C2) mangrove forest.

Parameters	Temala (n=24)			Coco (n=24)		
	Range	Average	SD	Range	Average	SD
Temperature	16.8-17.7	17.3	0.2	15.5-16.6	16.1	0.3
pH	7.7-7.9	7.8	0.1	7.6-8.0	7.7	0.1
Salinity	26.0-33.0	29.5	2.1	29.6-34.2	32.3	1.2

Table 2: Summary of the δD-S and δ^{18}O-S relationships in the Coco and Temala rivers during rain and dry seasons. Values in brackets show the r^2 values. The stable water isotope compositions of the Coco and Temala endmembers (δD_i and $\delta^{18}O_i$) were calculated by the extension of the δD-S and δ^{18}O-S relationships. For the Southeastern rivers and the marine endmembers, the δD_i and $\delta^{18}O_i$ values were calculated as the average of all river samples with salinity = 0 and the values recorded at station M, respectively. For the See text for more details.

	Endmembers	δD-S relationship	δ^{18}O-S relationship	δD_i (‰)	$\delta^{18}O_i$ (‰)	d-excess (‰)
Mangrove stations – Dry season	Coco (n=17)	y=2.1x–72.9 (0.8)	y=0.2x–9.9 (0.6)	-72.9±8.9	-9.9±1.7	15.8±1.3
	Temala (n=19)	y=1.0x–36.0 (0.9)	y=0.2x–8.4 (0.6)	-36.0±2.8	-8.4±1.2	15.9±2.9
Estuarine stations – Rain season	Temala and Coco (n=15)	y=1.0x–34.6 (0.9)	y =0.2x–5.0 (0.9)	-34.6±1.9	-5.0±0.4	0.4±5.8
	Marine (n=1)			-1.6±0.2	-2.1±0.2	
Freshwater stations	Southeastern rivers (n=14)			-31.2±6.2	-5.8±1.0	

Table 3: The fluxes ($R_i^{eff.}$, kg/yr) of REEs and Y from the two mangrove systems in New Caledonia (NC) and the extrapolation toward the global flux (ton, or Mg per year).

	Annual fluxes from mangroves in NC		Global flux
	Temala	**Coco**	
Y	16.1±4.6	6.1±1.3	42.1±21.2
La	6.2±1.2	2±0.6	14.8±7.6
Ce	6.4±1.7	3.9±1.3	22.8±14
Pr	1.1±0.3	0.4±0.1	3.0±1.5
Nd	5.5±1.1	1.8±0.4	13.3±5.6
Sm	1.2±0.2	0.4±0.1	2.9±1.4
Eu	0.3±0.1	0.1±0	0.8±0.7
Gd	1.6±0.4	0.6±0.3	4.2±3.3
Tb	0.3±0	0.1±0.03	0.6±0.3
Dy	1.8±0.4	0.6±0.2	4.5±2.7
Ho	0.4±0.1	0.1±0	1.0±0.6
Er	1.1±0.3	0.5±0.2	3.1±1.8
Tm	0.1±0.03	0.1±0.02	0.4±0.3
Yb	0.8±0.3	0.4±0.2	2.4±2.5
Lu	0.1±0.03	0.05±0.01	0.3±0.2